Oil & Natural Gas Technology

DOE Award No.: DE-FE0010144

Final Scientific/Technical Report

Mapping Permafrost and Gas Hydrate using Marine CSEM Methods

Project Period (10/1/2012 – 09/30/16)

Submitted by:
Project PI Steven Constable
Scripps Institution of Oceanography
University of California San Diego
DUNS #:175104595.
9500 Gilman Drive
La Jolla, CA 92093-0210
e-mail: sconstable@ucsd.edu
Phone number: (858) 534-2409

Prepared for:
United States Department of Energy
National Energy Technology Laboratory

Steven Constable

Digitally signed by Steven Constable
DN: cn=Steven Constable, o=UCSD, ou=IGPP/SIO, email=sconstable@ucsd.edu, c=US
Date: 2016.12.13 08:14:42 -08'00'

Office of Fossil Energy

Acknowledgment: “This material is based upon work supported by the Department of Energy under Award Number DE-FE0010144.”

TABLE OF CONTENTS Page

EXECUTIVE SUMMARY 1
INTRODUCTION 2
CONSTRUCTION AND TESTING OF INSTRUMENTATION 3
DATA COLLECTION 11
CSEM SURVEY RESULTS 15
INTERPRETATION AND CONCLUSIONS 34
RESEARCH PRODUCTS 35
APPENDIX 36
REFERENCES 44

EXECUTIVE SUMMARY

Permafrost underlies an estimated 20% of the land area in the northern hemisphere and often has associated methane hydrate. Numerous studies have indicated that permafrost and hydrate are actively thawing in many high-latitude and high-elevation areas in response to warming climate and rising sea level. Such thawing has clear consequences for the integrity of energy infrastructure in the Arctic, can lead to profound changes in arctic hydrology and ecology, and can increase emissions of methane as microbial processes access organic carbon that has been trapped in permafrost or methane hydrate dissociates. There has, however, been significant debate over the offshore extent of subsea permafrost.

Our knowledge of sub-seafloor geology relies largely on seismic data and cores/well-logs obtained from vertical boreholes. Borehole data are immensely valuable (both in terms of dollar cost and scientific worth), but provide information only about discrete locations in close to one (vertical) dimension. Seismic data are inherently biased towards impedance contrasts, rather than bulk sediment properties. In the context of mapping offshore permafrost and shallow hydrate, seismic methods can identify the top of frozen sediment through the identification of high amplitude reflections and high-velocity refractors but simple 2D seismic surveys do little to elucidate the bulk properties of the frozen layers, particularly the thickness. However, permafrost and gas hydrate are both electrically resistive, making electromagnetic (EM) methods a complementary geophysical approach to seismic methods for studying these geological features. Deep ocean EM methods for mapping gas hydrate have been developed by both academia and industry, but the deep-ocean techniques and equipment are not directly applicable to the shallow-water, near-shore permafrost environment. During this project this problem was addressed by designing, building, and testing an EM system for very shallow water use, and using it to not only contribute to the understanding of the extent of offshore permafrost, but also to collect baseline data that will be invaluable for future studies of permafrost degradation.

We used the new equipment to carry out a pilot project to map the contemporary state of subsea permafrost on part of the U.S. Beaufort inner shelf. Our towed array was 1000 m long and contained four equally spaced receivers. The towed array was supplemented by the deployment of 3 moored seafloor receivers that were retrieved after the cruise so that nothing remains in the area. We see permafrost as a 60-100 Ωm vertically resistive anomaly with high anisotropies to depths of 600 m, thinning west and thicker in the region of the Sag River outflow. High anisotropies are required to simultaneoulsy fit amplitude and phase data. By using a second geophysical method to supplement seismic data, we were able to better map the current extent of permafrost and provide a critical baseline for studies which target the effects of current climate change.

Instrumentation and analytical methods developed for this project can be easily applied for future permafrost and hydrate mapping elsewhere, and also for applications such as groundwater exploration and engineering studies associated with near-shore infrastructure development, and most recently offshore geothermal exploration.

1 Introduction

Temperatures cold enough to form permafrost have been present in the Arctic since the end of the Pliocene (about 1.9 Ma) and as a result permafrost underlays roughly 20% of land in the northern hemisphere (*Collett et al.*, 2011). Permafrost is defined as ground that has been held at or below 0°C for at least two years, "ice-bearing" specifies that the pore spaces contain a mixture of ice crystals and pore fluid while "ice-bonded" describes cementation of sediment grains (*Osterkamp*,2001). Over the last 20,000 years sea level has risen 120 m and submerged portions of Arctic coastline and permafrost. The warm, saline conditions introduced by sea level rise are causing the relict subsea permafrost to thaw (*Osterkamp*,2001). The maximum extent of permafrost offshore, therefore, is the 120 m isobath (*Collett et al.*, 2011), but current seismic studies suggest that permafrost does not extend beyond the 20 m isobath (*Brothers et al.*,2012).

Permafrost often has associated gas hydrate, which requires low temperature and high pressures to be stable and typically exists beneath the deep ocean floor. However, consistent cold ground temperature in the presence of ice-bearing permafrost allows gas hydrate to currently exist on land and in shallow water environments. Without the permafrost cap to thermally stabilize them, hydrates could dissociate and release their bound methane gas, affecting future climate change.

Prior studies conducted on the Beaufort Shelf, Alaska, have used the seismic refraction method to infer extent of permafrost. Seismic refraction uses the increase in P-wave velocity (V_p) due to ice in pore spaces to determine the presence of permafrost. Theory predicts a V_p of 2.5 - 2.8 kms^{-1} for sands with less than 40% ice saturation, and above 40% saturation a sharp jump in seismic velocity to between 3.4 and 4.35 kms^{-1} due to the onset of cementation of sediment grains (*Johansen et al.*, 2003). In the Beaufort Sea velocities varied between 1.7 - 4.6 kms^{-1} with all permafrost layer refractions (PLRs), defined as $V_p > 2.3$ kms^{-1}, occurring within 30 km of the coast and shallower than 20 m water depth (*Brothers et al.*, 2012).

Although PLRs can be used to define the lateral extent of permafrost, the seismic method has difficulty determining depth boundaries and bulk properties of permafrost (*Brothers et al.*, 2012). The velocity contrast at the top boundary is so large that most of the seismic energy does not propagate beneath it. The bottom permafrost boundary is likely diffuse and is a velocity decrease, both of which result in a weak or non-existent refraction signal. As a consequence, the seismic method can image the top of the permafrost layer at best. Additionally, the refraction method cannot differentiate between frozen and unfrozen fine grained sediments, which means the depth obtained from this method may not be the top of the permafrost layer if fine sediments overly coarse ones (*Brothers et al.*, 2012).

Electromagnetic methods complement seismic data by resolving the top and bottom boundaries, as well as estimating the volume fraction of permafrost. CSEM is sensitive to the resistivity increase caused by ice forming in pore spaces, as well as to the resistivity

decrease below the permafrost as the sediments transition to an unfrozen state. Onshore boreholes have measured ice-bonded permafrost with resistivities from 100 Ωm to over 1000 Ωm to depths of 660 m near the coast of Prudhoe Bay (*Collett et al.*, 1989). Below the permafrost layer resistivities drop to between 5 and 15 Ωm (*Collett et al.*, 1989). We expect the resistivity of offshore ice-bearing permafrost to be lower than the measured onshore values because of intrusive saline pore fluids *Daniels et al.*, 1976). Land borehole measurements of hydrate beneath permafrost in the Eileen accumulation, located near the coastline just west of Prudhoe Bay, reach 2000 Ωm at a depth of about 600 m (*Collett et al.*, 2011). Gas hydrate occurs at greater depths and has a higher resistivity than permafrost, and so with careful interpretation one might be able to distinguish between the two.

2 Construction and testing of instrumentation

Instruments were designed to operate in the shallow water (<10 m) of the Beaufort shelf, details of all instrument designs are in the section below. The entire system is light and small enough to be easily air freighted, transported in one load using a utility vehicle, and operated off a small (16 m) fishing boat. This makes it a relatively easy and inexpensive system to operate, and it has already been used for a number of other applications including groundwater and geothermal exploration in the Atlantic and Gulf of California, respectively (e.g., *Martin*, 2015).

2.1 Instruments Develped

Final tranmitter design is shown in Figure 1. The transmitter operates off 110 VAC power and is capable of 50 amps output, in the form of an arbitrary GPS stabilized ternary waveform, on a 50 m antenna. Upgrades to the final design include the ability to generate a current controlled output and packaging the power supply with an integrated GPS clock into one complete unit. Laptop with read out of temperature, current, and voltage along with a backup GPS clock are strapped on top of the transmitter unit to monitor its output in real time.

A schematic of the final towed receiver design is shown in Figure 2. We named the receivers Porpoises because of how they occasionally leap from the water when encountering ice. Inline electric field was measured on a 2 m dipole held .67 m underwater in a rigid fiberglass boom. As with the Vulcan instruments, we chose rigid antennas instead of cable arrays to avoid motional noise associated with cable motion through Earth's magnetic field (*Constable et al.*, 2016). The data logger within the plastic case records inline electric field, acceleration in three directions, and a timing pulse sent from an external GPS receiver. GPS receivers are attached to the top of the Porpoises on short masts and a serial data logger within the logger package records time and location. A second serial data logger records pitch, roll, and heading from a compass/tiltmeter every second. Images of the Porpoises used in the Arctic are shown in Figure 3.

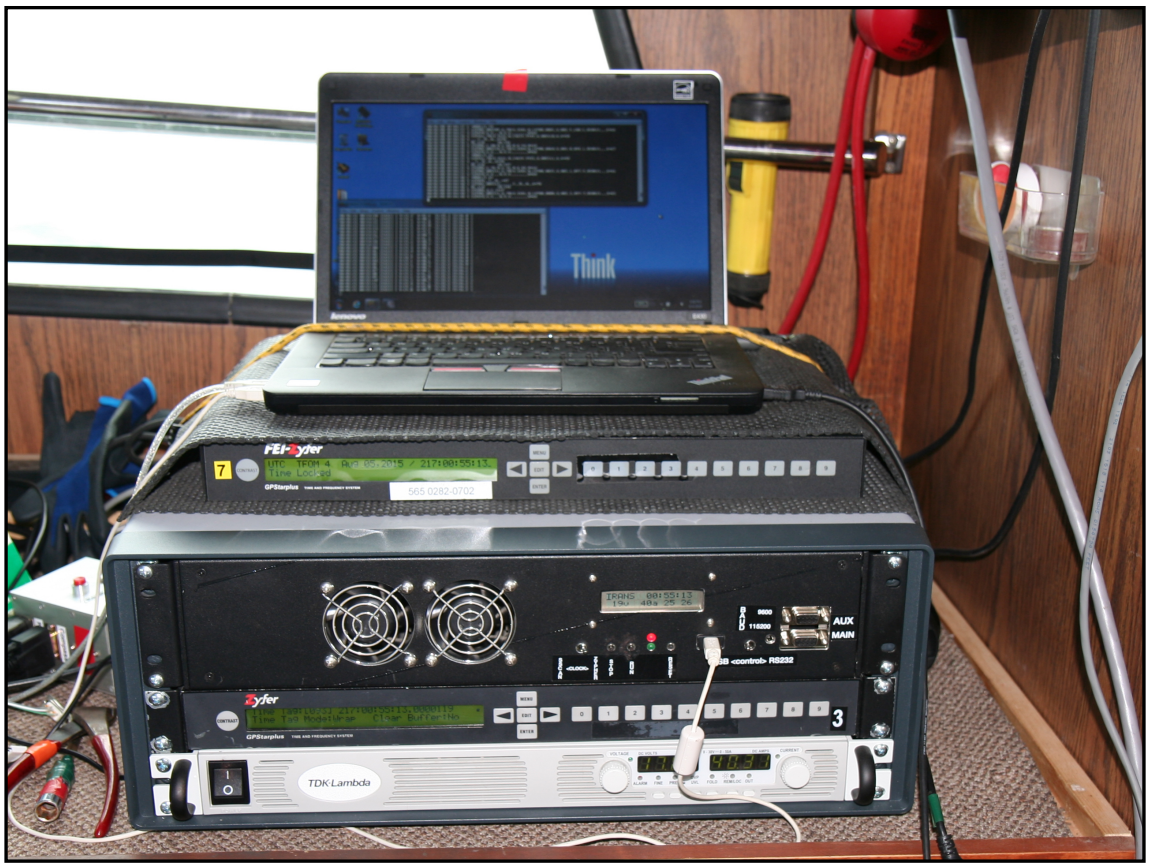

Figure 1: Compact tranmitter, operates off 110VAC and capable of constant current output of up to 50 amps on a 50 meter antenna.

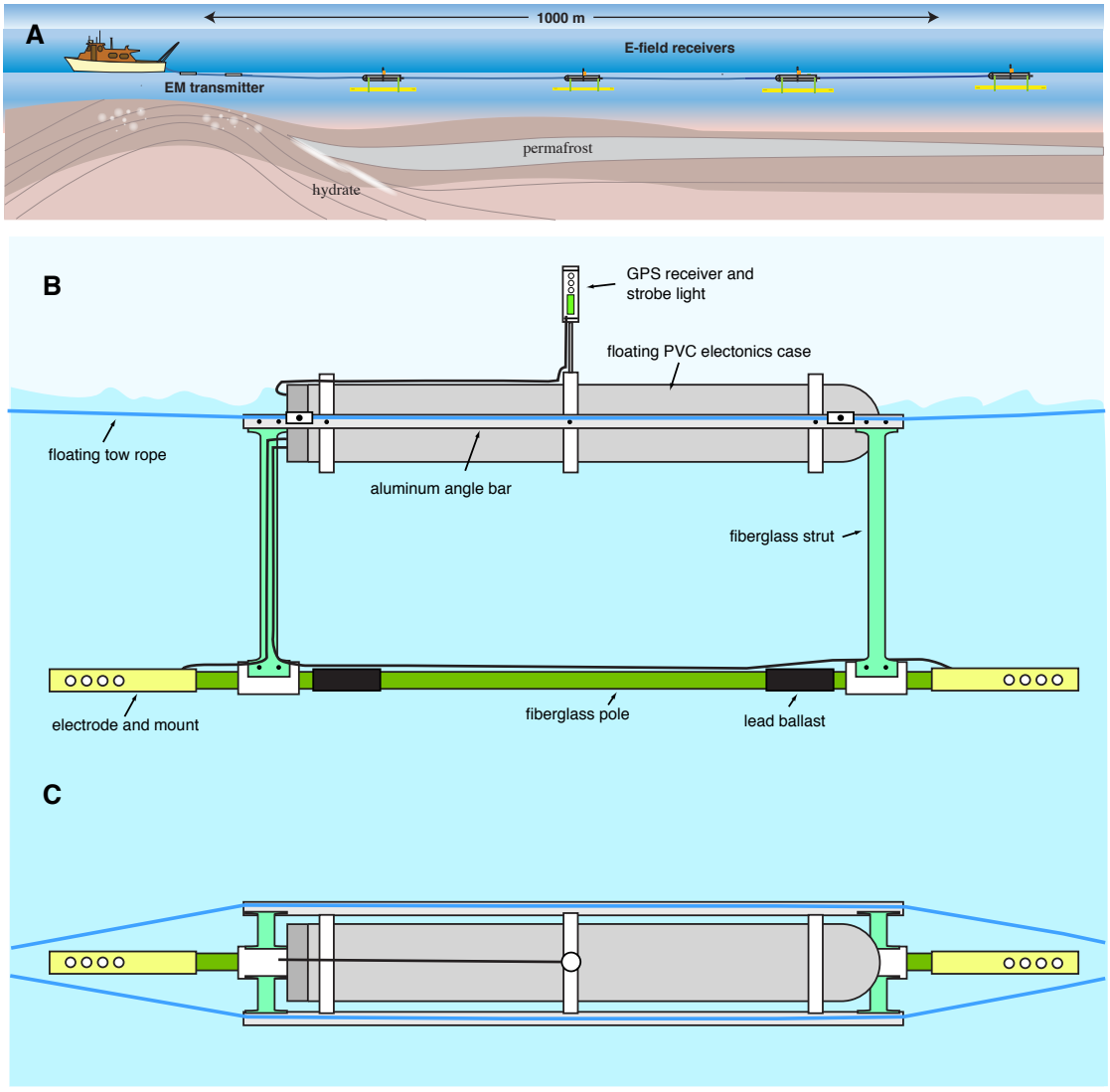

Figure 2: A: Surface-towed Porpoise array. Multiple receivers are easily clipped into the tow rope during deployment. B: Side view schematic of a Porpoise receiver. C: Plan view of a Porpoise receiver.

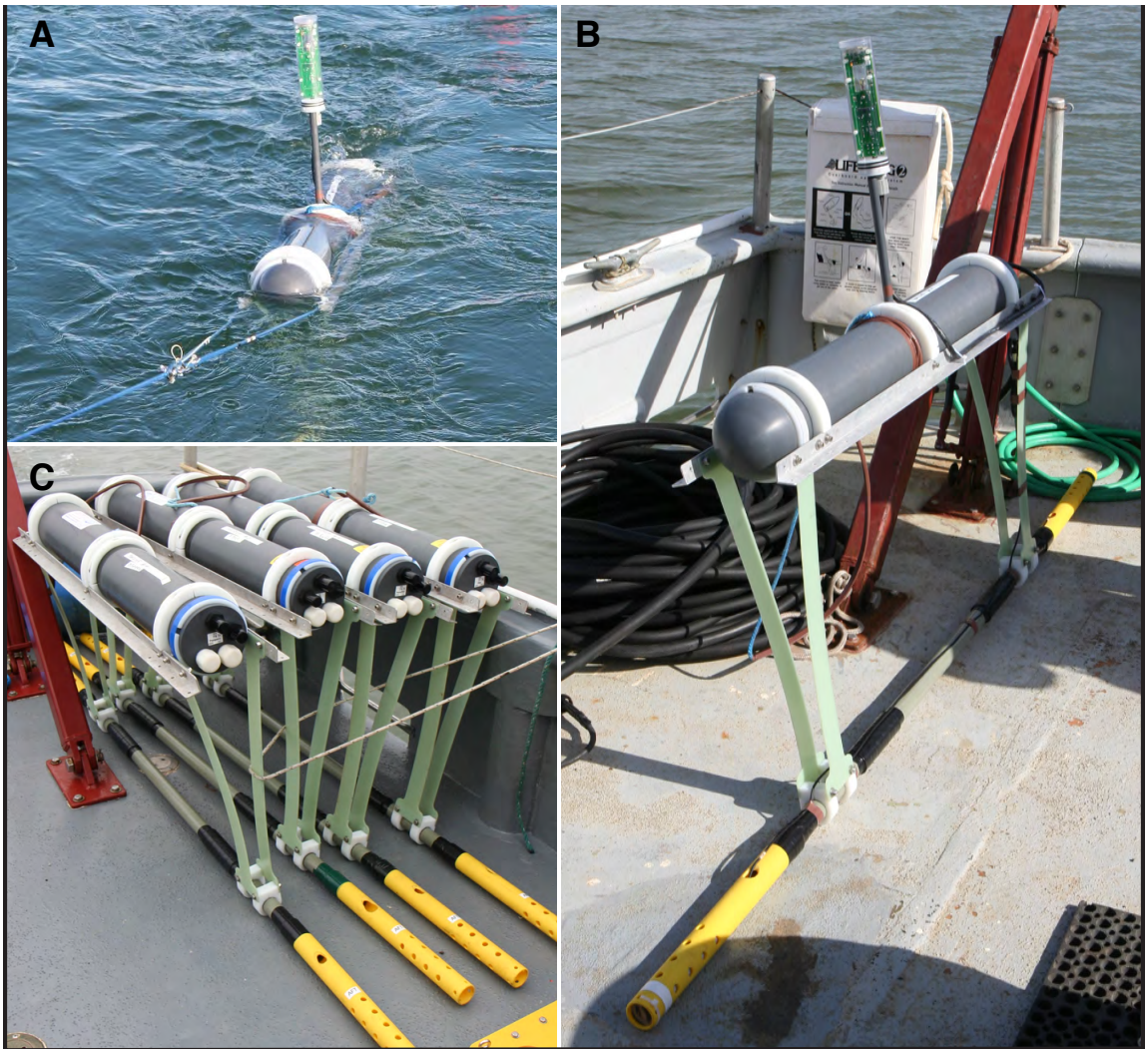

Figure 3: A: Porpoise floating on the surface after being deployed. B: Porpoise ready to be deployed. C: All four Porpoises stored on deck, electrodes and GPS receivers still need to be attached.

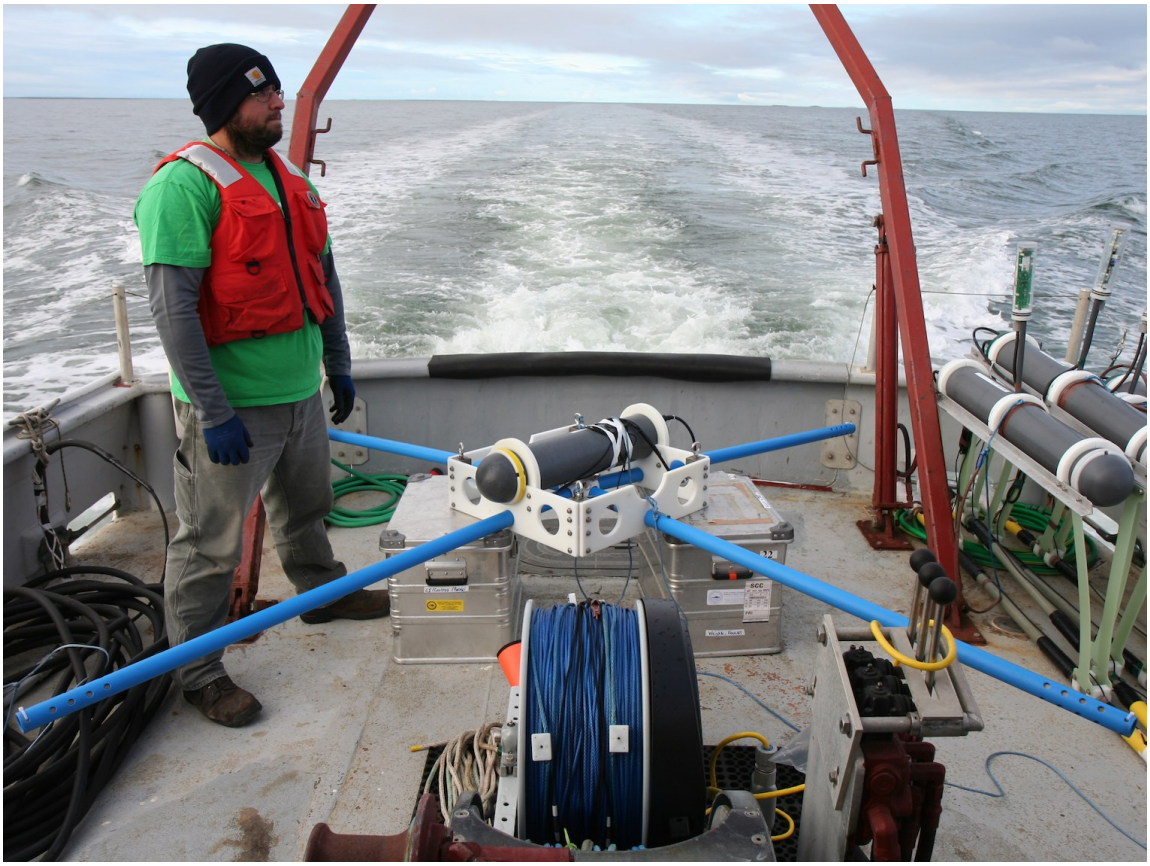

Figure 4: Moored seafloor receiver ready to be deployed off the deck of the R.V. Ukpik.

Towed receivers were supplemented with a few seafloor receivers. These receivers were moored with roughly 20 lbs of lead weight and attached to a buoy so that they could be found and retrieved. Nothing was left behind on the seafloor after retreaval. Seafloor receivers measured two orthogoal directions of the electric field on 10 m dipoles and data were recorded using the same amplifier logger as the towed receivers. An external compass recorded receiver orientation every hour. An image of a seafloor receiver ready to be deployed is shown in Figure 4.

A conductivity, temperature, and depth (CTD) profiler was towed alongside the vessel to constantly measure the surface (depth <1 m) water conductivity. When towing into deeper water the CTD was lowered to the seafloor slowly to obtain a vertical profile. This was done a total of 12 times after the vessel was stopped and porpoises recovered. The ocean water conductivity was variable due to influx of freshwater from river outflows and melting sea ice. Data from the CTD were incorporated in data processing to prevent these variations from influencing the subsurface resistivity strutures.

2.2 Porpoise Noise

Power spectra for the Porpoise receivers were calculated over a 10 min window using data collected during our engineering test cruise offshore San Diego. During this 10 min window the Porpoises were towed through the water with the transmitter turned off. At 1 Hz noise levels are on the order of a few microvolts and at 30 Hz the noise contributes tens of nanovolts. The peak centered around 0.3 Hz is due to wave noise or strumming of the instrument. The noise spectra is compared to published values for the Vulcan receiver and the traditional ocean bottom receivers (*Constable et al.*, 2016). The Porpoise receiver has the highest noise floor, which is to be expected due to the increased wave motion at the surface.

We conducted synthetic forward modeling to determine the offsets and frequencies most sensitive to permafrost, modeled as a 200 m thick layer of 100 Ωm material buried at a depth of 200 m in 1 Ωm marine sediment. This model was intentionally chosen to be conservative and was constructed based on modelling and well log data (*Osterkamp*, 2001). Forward responses were calculated for the permafrost model as well as a halfspace of pure sediment. In both cases water depth was 5 m and the calculation was done for offsets of 100 to 1100 m and frequencies of 1 to 40 Hz. Figure 6 shows (A) the amplitude of the permafrost model response normalized by the halfspace response and (B) the difference in model phases. Largest sensitivity to a permafrost layer occurs at offsets longer than 500 m and at frequencies less than 30 Hz.

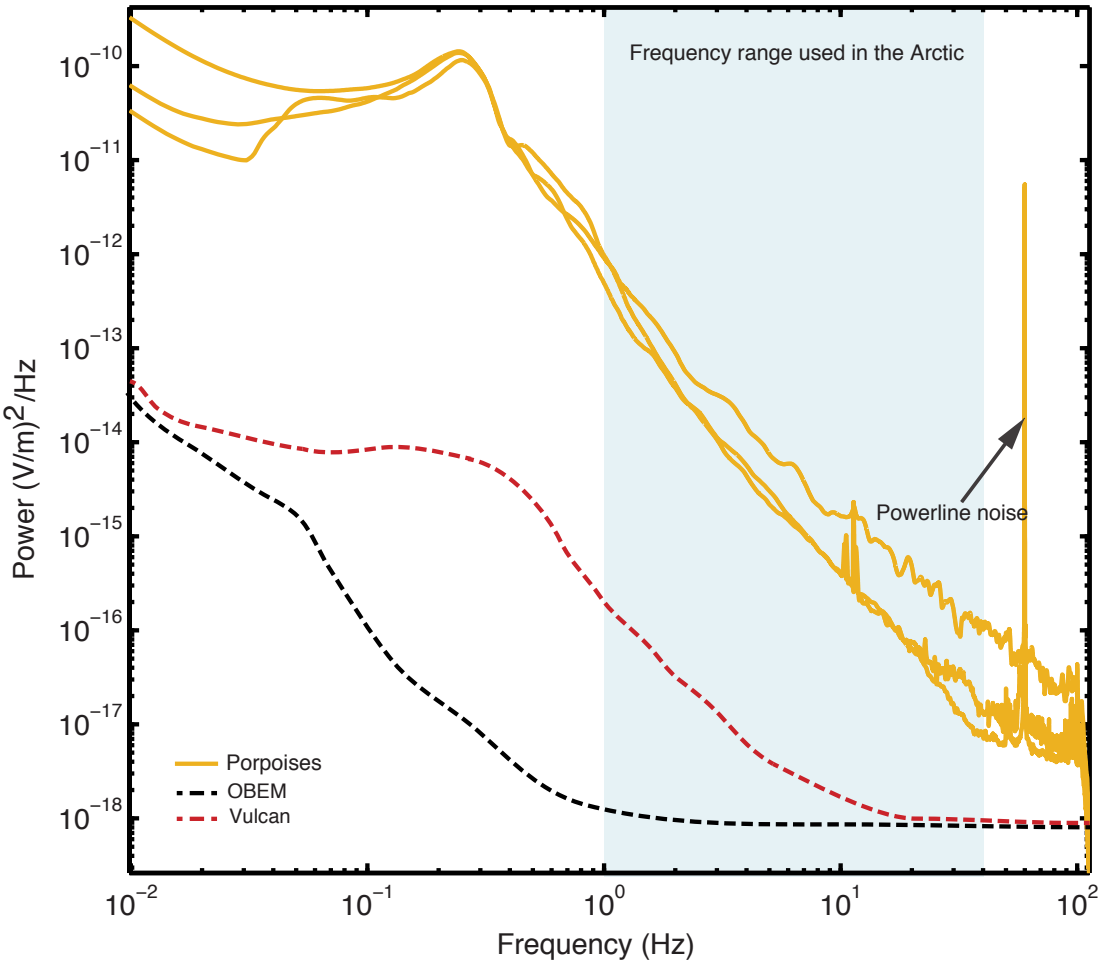

Figure 5: Power spectra of various EM receivers. Porpoise data were collected on a test cruise offshore San Diego in May of 2014. Vulcan and OBEM spectra are from (*Constable et al.*, 2016) and are shown as broken lines.

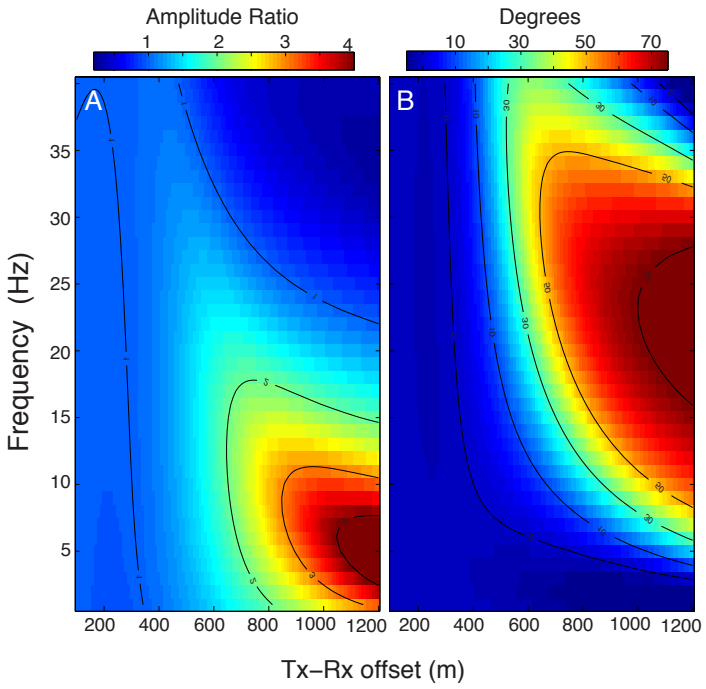

Figure 6: A: Amplitude anomaly or permafrost model amplitude normalized by a 1 Ωm halfspace amplitude. An amplitude anomaly of 1 indicates no difference. B: Phase anomaly or phase difference between the two models. The permafrost model was a 200 m thick permafrost layer with 100 Ωm resistivity buried at a depth of 200 m in 1 Ωm sediments.

3 Data collection in the Arctic over two years

Our survey was conducted over the course of two years, in 2014 for five days from July 16-22 and in 2015 for seven days from July 29 - August 6. A total of 365 km of data, 153 km in 2014 and 212 km in 2015, were towed. Research was conducted off the R.V. Ukpik out of West Dock, Prudhoe Bay, AK. Figure 7 shows lines collected during both years of survey. The coast was covered from Harrison Bay to east of the Sagavanirktok (also called the Sag) River outflow. Our ability to collect data offshore was limited by the presence of sea ice, which prevented towing beyond the barrier islands both years.

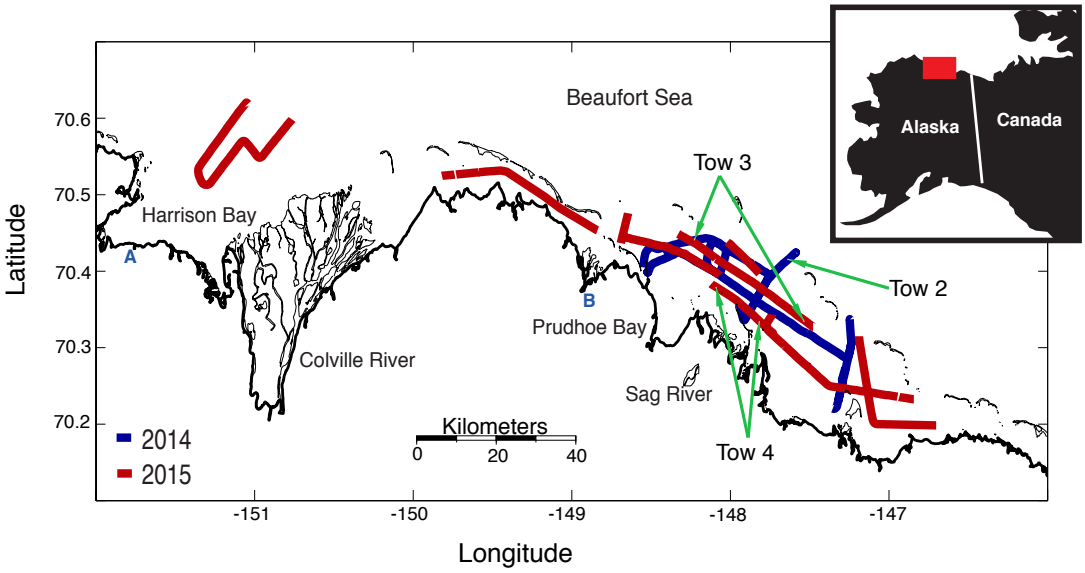

Figure 7: Map of survey area with lines collected during both 2014 and 2015 displayed. (A) is the location of an onshore borehole near Harrison Bay and (B) is the location of an onshore borehole near Prudhoe Bay.

Based on the sensitivity analysis from Figure 6, we decided to tow at low frequencies and long offsets. In our survey design Porpoises were towed at 250, 500, 750 and 1000 m offsets, we find that including a shorter range Porpoise helps constrain the shallow sediment and ultimately helps resolve permafrost in inversions of the data. The array was kept at 1 km in length for logistical reasons. We transmitted a 1 Hz fundamental of Waveform-D, a modified square wave that spreads power from the fundamental frequency into higher odd harmonics spanning at least one decade (*Meyer et al.*, 2010). Data were processed for the fundamental (1 Hz) and odd harmonics out to 33 Hz, but only the three largest harmonics (3 Hz, 7 Hz, and 13 Hz) were ultimately included in inversions.

All time series recorded by Porpoise and seafloor receivers were Fourier transformed and stacked into 60 second windows (*Meyer et al.*, 2010). Stacking the data increases its statistical reliabliity and provides estimates of error bars, which are used as inputs to our inversion algorithm. Figures 8 through 10 show stacked data samples of porpoises from both years and a seafloor receiver from 2015. It is easier to see variations in Porpoise data because they are fixed offset, an increase in amplitude typically corresponds to resistive structure and decreased amplitude conductive structure. The seafloor receiver amplitudes fall off with increasing range. Data up to 6 km range were processed successfully and inverted from seafloor receivers.

There was a timing issue during the first year of the survey, rendering all phase data from 2014 not useable. This was fixed in 2015 by sending a GPS pulse to the towed receivers that was used to correct crystal clock drift.

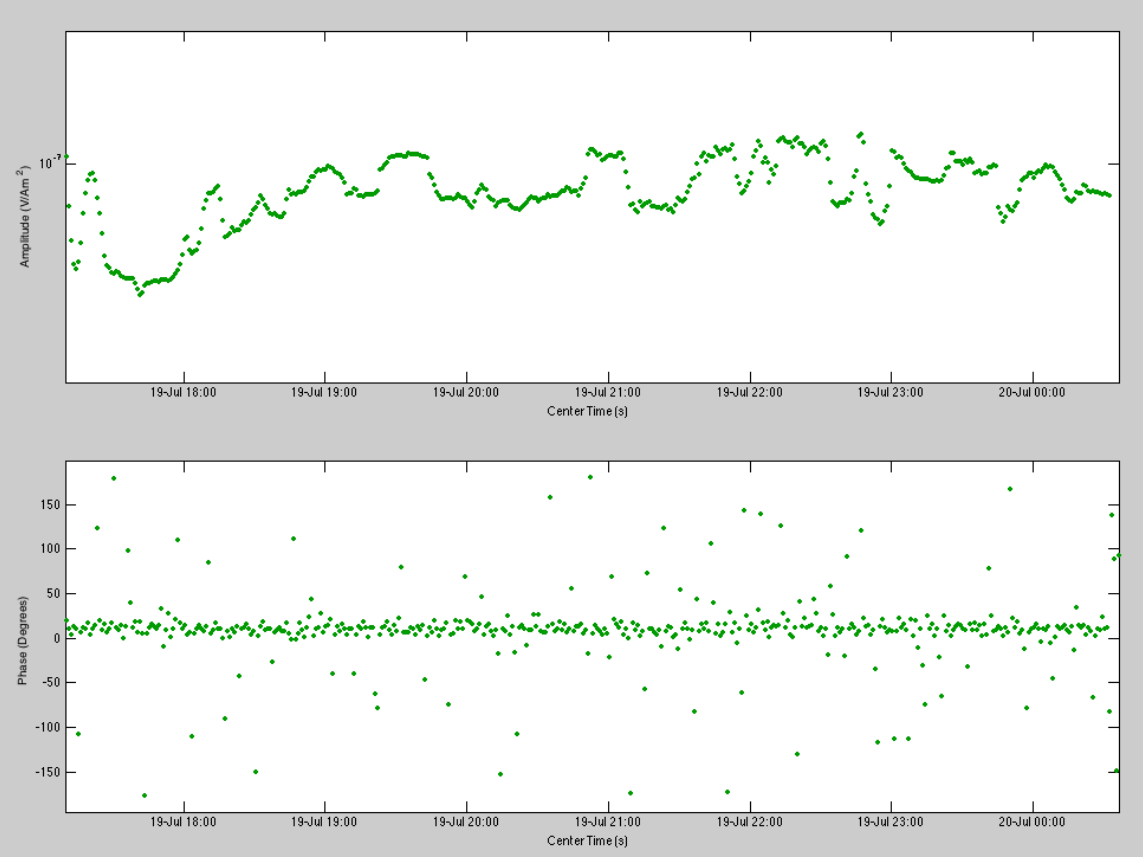

Figure 8: Example data from 250 m offset Porpoise in 2014 at 3 Hz. Phase data is not useable.

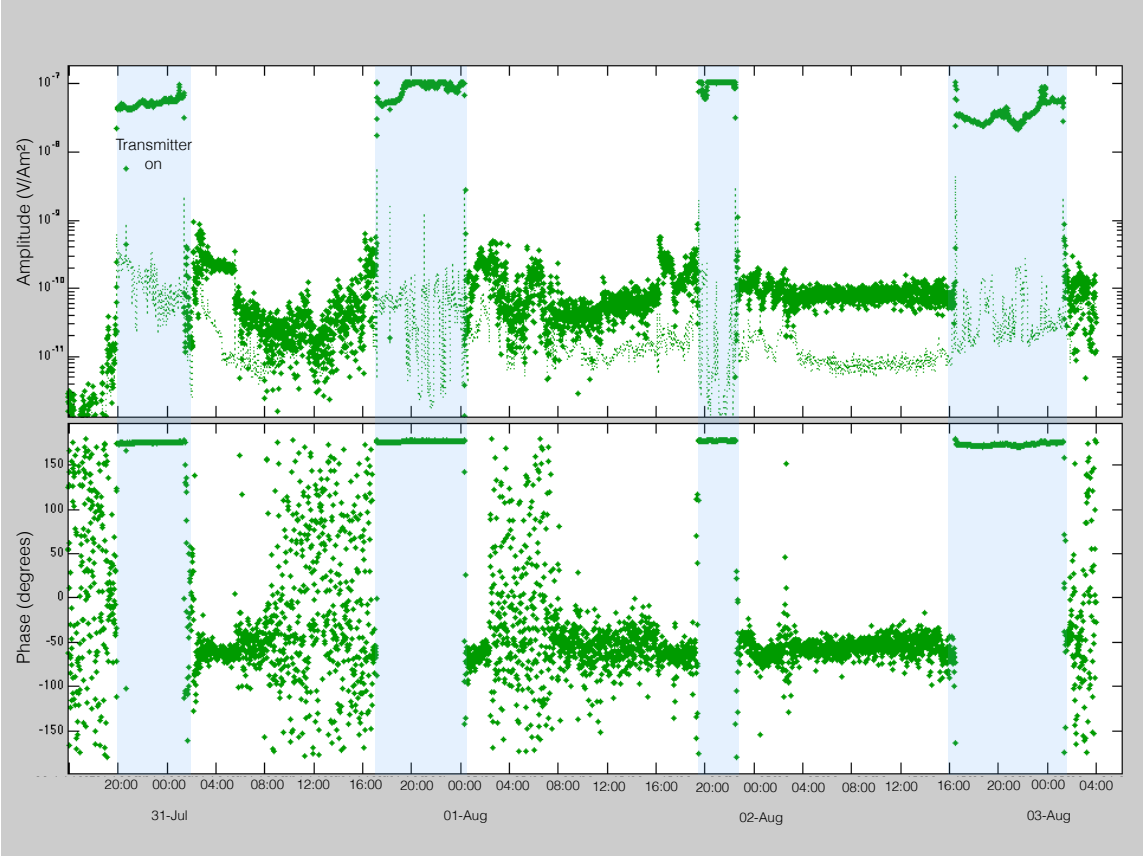

Figure 9: Example data from 250 m offset Porpoise in 2015 at 3 Hz, multiple tows present. Times when transmitting are highlighted in blue.

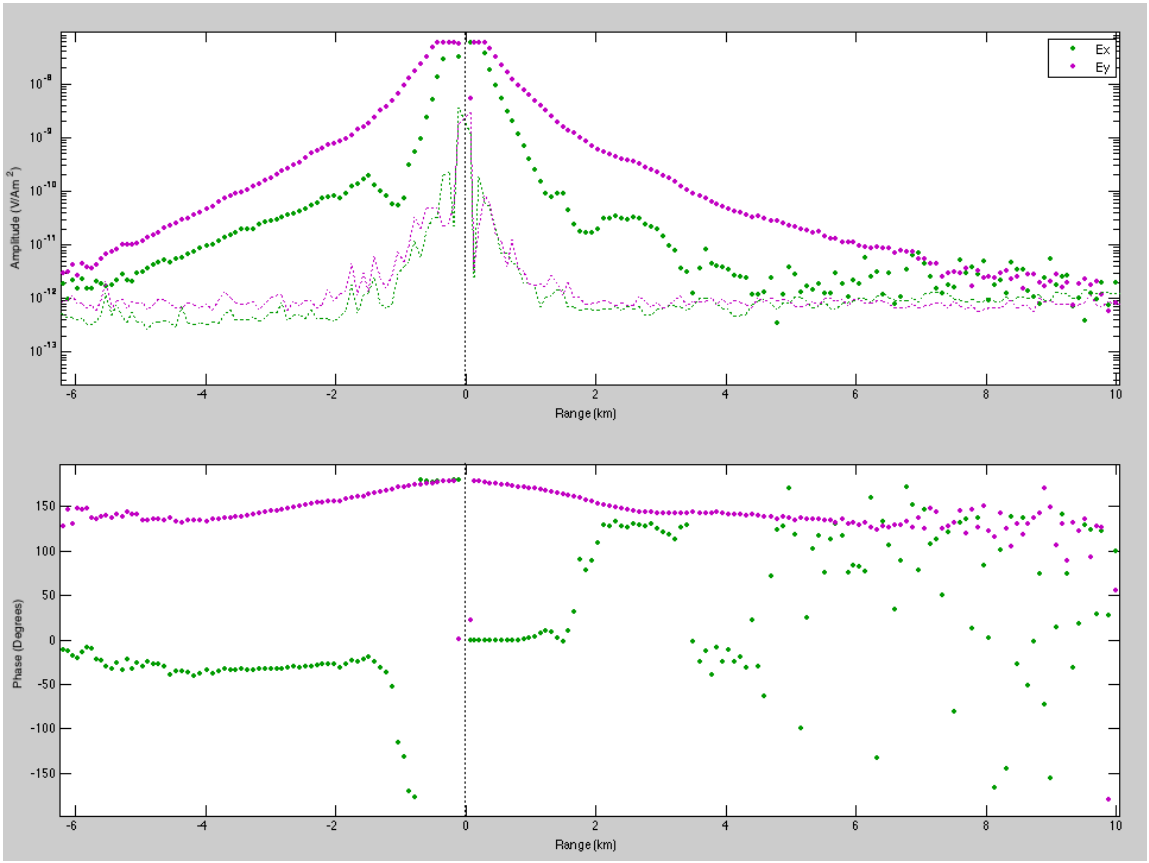

Figure 10: Example data from seafloor receiver in 2015 at 3 Hz, rotated so that magenta is inline and green is crossline.

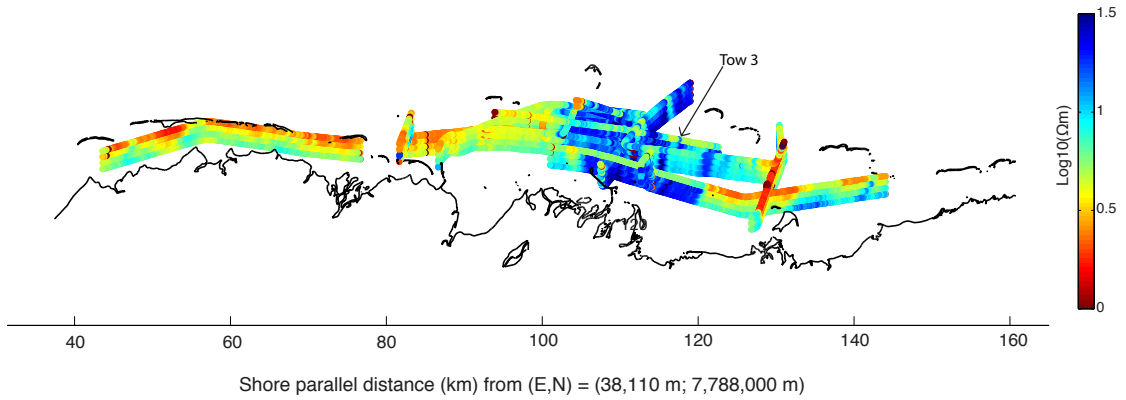

Figure 11: Fence diagram of offset apparent-resistivity pseudosections offshore Prudhoe Bay and the Sagavanirktok (Sag) river outflow for both years computed for 3 Hz amplitudes. Blue corresponds to higher resistivity values (up to 30 Ωm) while red is more conductive (down to 1 Ωm).

4 CSEM survey results

We created pseudosections by calculating the forward solution for 1D models, including appropriate water depth from an echosounder and seawater conductivity from CTD measurements, underlain by halfspaces ranging from 0.1 to 1000 Ωm and interpolating to find the best resistivity for each value of stacked amplitude. Pseudosections are useful for displaying the lateral variability of a data set, but have limited ability to determine depths (*Weitemeyer et al.*, 2006). The pseudosections for a frequency of 3 Hz are shown in Figures 11 and 12, short offsets are plotted as shallow structure and long offsets as deeper structure.

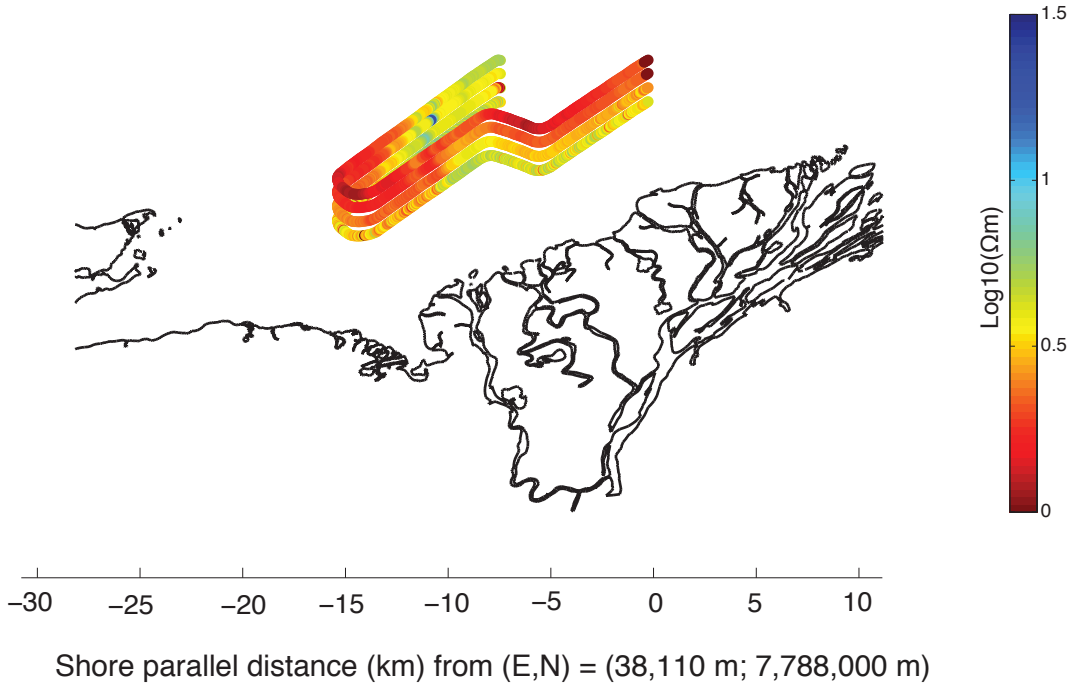

Figure 12: Fence diagram of offset apparent-resistivity pseudosection in Harrison Bay and near the Colville river outflow computed for 3 Hz amplitudes.

The offset pseudosections (Figures 11 and 12) show significant lateral variability in permafrost extent. Harrison Bay appears very conductive with highest resistivities near 10 Ωm, which is unexpected given that permafrost is seismically inferred in this area (*Brothers et al.*, 2012). However, it is consistent with well logs that show thinning of the ice bearing permafrost layer onshore to the west of Prudhoe Bay (*Collett*, 1989). Onshore at Harrison Bay a well log (labelled A in Figure 7) measures maximum resistivity near 100 Ωm down to 120 m, where resistivity drops to over 10 Ωm and the base of the ice-bearing layer is seen at 300 m (*Collett*, 1989). If most of the 120 m thick resistive layer has thawed, the underlying permafrost would be consistent with resistivity values in the pseudosection. Along the coast between Harrison Bay and Prudhoe Bay there is a clear layer of conductive sediments overlying a buried layer of more resistive material, interpreted as permafrost. Just east of Prudhoe Bay there is an increase in resistivity at all depths, implying that permafrost is pervasive in the area near the Sagavanirktok (also called the Sag) River outflow. Because of freshwater influx from rivers and melting of sea ice, sea water conductivity was variable across the entire survey area. In the top meter ocean conductivity ranged from 0.3 to 0.5 Ωm, but at depth remained more constant near 0.4 Ωm. Seawater conductivity variations and water depth were included in the 1D model layers used for pseudosections and therefore do not cause the apparent resistivity variations.

4.1 Inversions

Inversions were done using the MARE2DEM adaptive refinement finite element code (*Key*, 2016). Amplitude only isotropic inversions were run for all tow lines as a starting point. Reasonable misfits were achieved for a 3% noise floor on all tow lines in 2015. Once phase was added, however, most inversions could not converge using an isotropic model and anisotropy was needed to fit the phase data. All inversions were limited to the three largest harmonics of Waveform-D (3, 7, and 13 Hz) for the first three Porpoises (offsets of 250, 500, and 750 m) and the largest two harmonics (3 and 7 Hz) for the last 1000 m offset Porpoise. The inversion grid sizes range from quadrilaterals 150 m wide by 10 m deep in the shallowest region up to 250 m by 50 m at greater depths. The increasing grid size is meant to mimic the loss of spatial resolution with depth as well as decrease computational resources. Due to the variation in water conductivity, we allowed a 2-layer ocean model be free parameters in the inversion, bounded by the maximum and minimum values that were measured with our towed CTD.

We will use Tow 3 as an example to demonstrate the differences in results for isotropic amplitude only inversions, isotropic amplitude and phase, and anisotropic amplitude and phase. Tow 3 is the long tow line from 2015 that begins west of the Sag River and continues until its eastern edge, it is labelled in Figures 7 and 11. The isotropic amplitude only model fits the data to an RMS of 1.5 with a 3% noise floor and is shown in Figure 13 along with a comparison between data and model prediction in Figure 14.

The inversion for Tow 3 including both amplitude and phase in an isotropic model

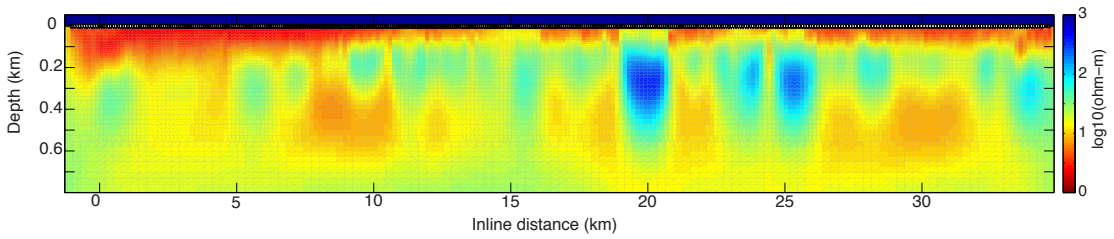

Figure 13: Amplitude only isotropic inversion from Tow 3 in 2015. RMS 1.5 with a 3% noise floor.

space did not reach a misfit below 2.6, still with a 3% noise floor, and the phase data had a consistent offset, producing biased residuals. The inversion and model fit to data can be found in Figures 15 and 16, respectively. Allowing for anisotropy improves the model fit to an RMS of 1.3 with a 3% noise floor, better even than the ampliutde only inversion. The anisotropic inversion is found in Figure 17 and its model fit in Figure 18. A comparison of residuals can be found in Figure 19, where it is clear that anisotropy makes the residuals less biased.

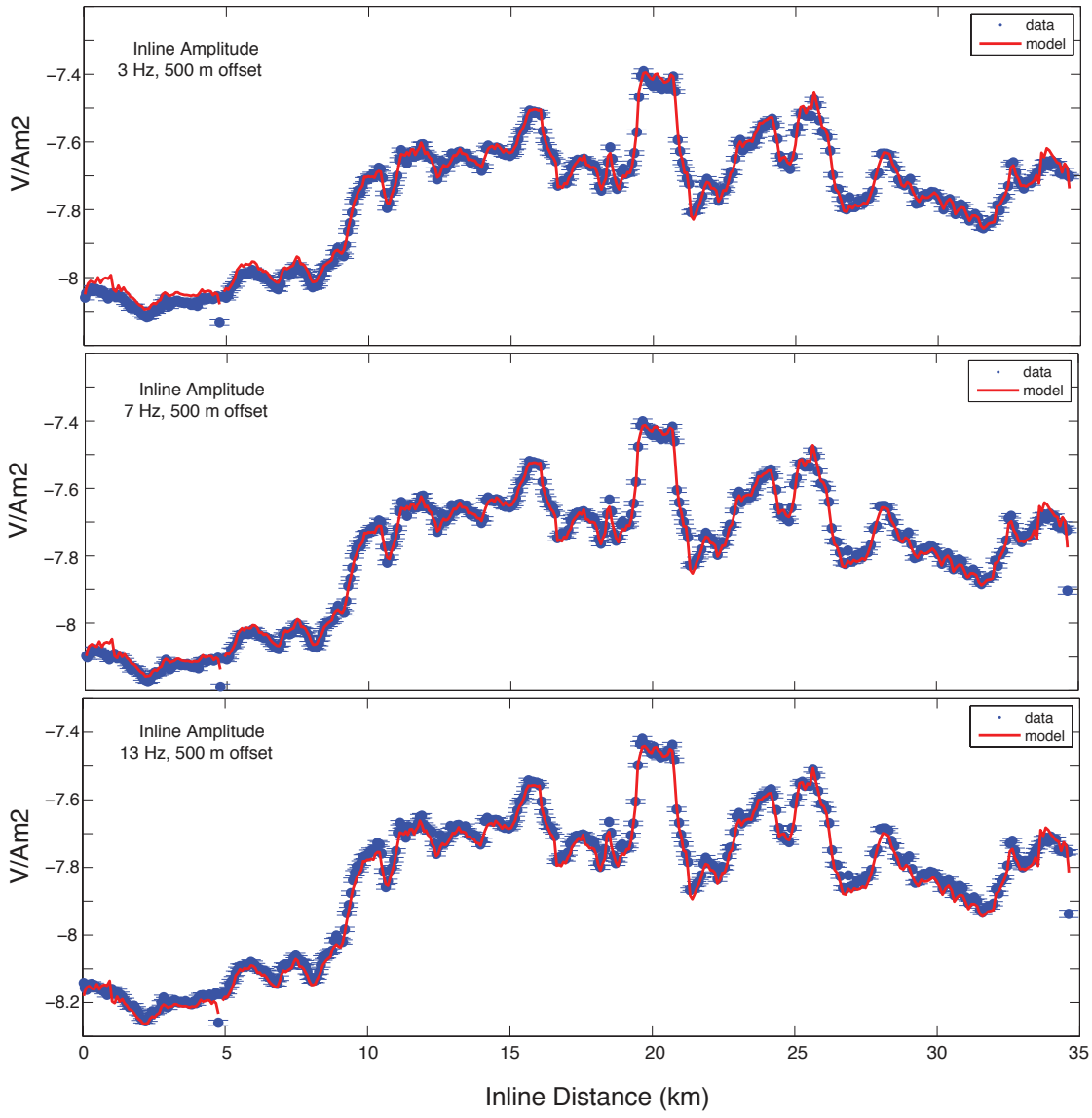

Figure 14: Line fits of data and model response from amplitude only isotropic inversion at 3, 7, and 13 Hz from Tow 3 in 2015, 500 m offset Porpoise.

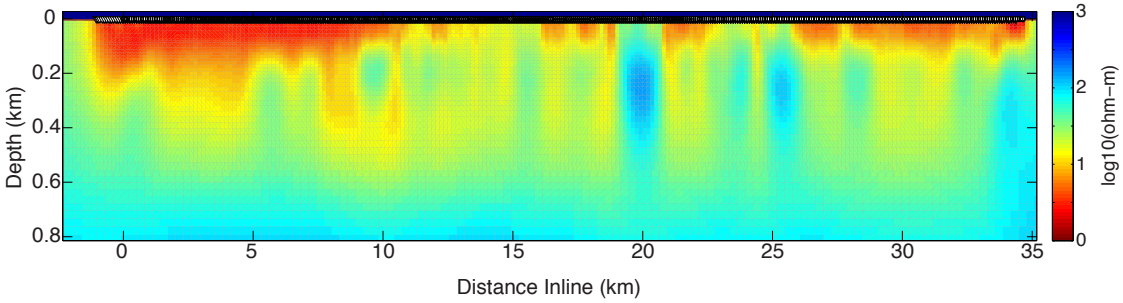

Figure 15: Amplitude and phase isotropic inversion from Tow 3 in 2015. RMS did not reach below 2.6.

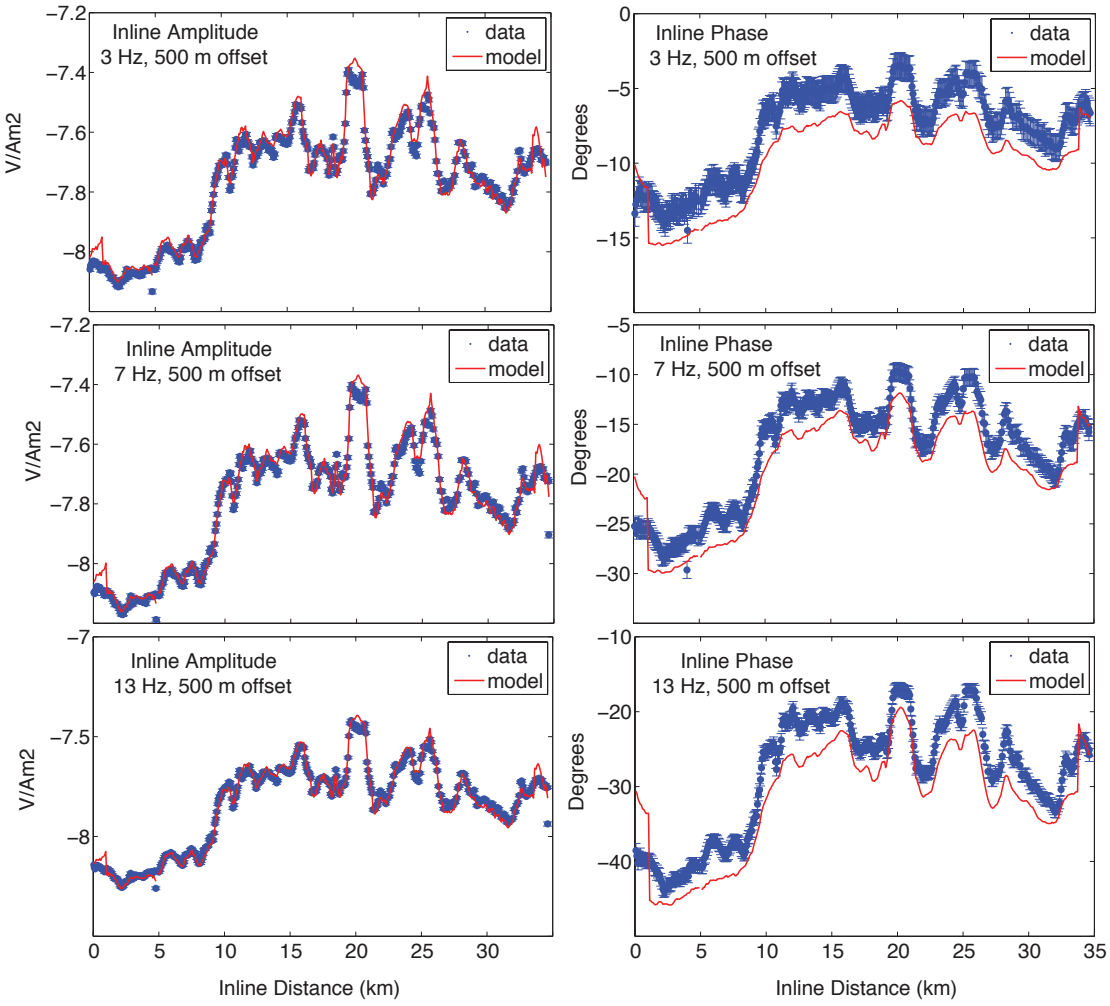

Figure 16: Line fits of data and model response from amplitude and phase isotropic inversion at 3 Hz from Tow 3 in 2015, 500 m offset.

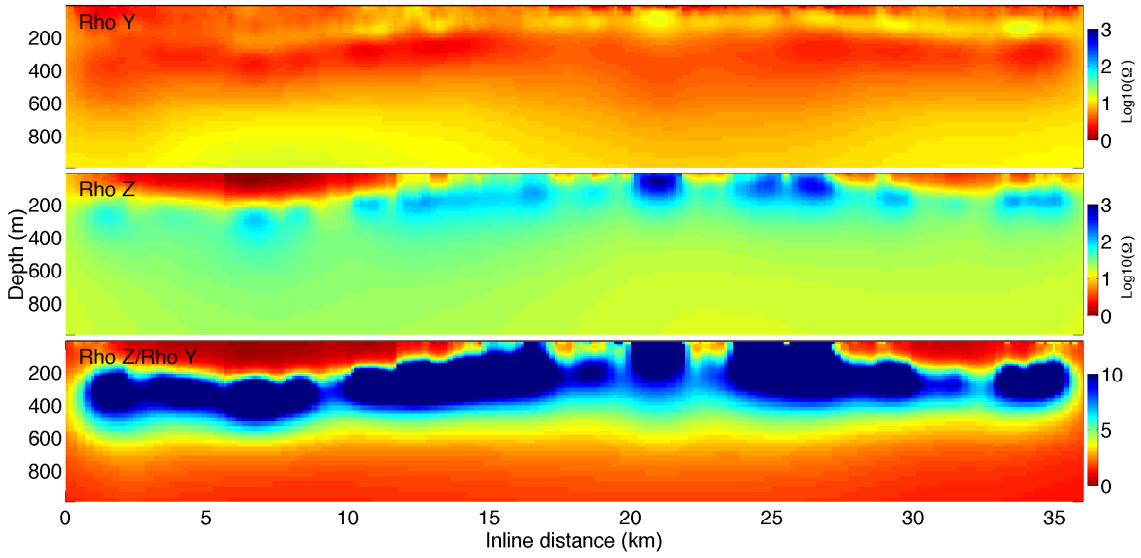

Figure 17: Amplitude and phase anisotropic inversion from Tow 3 in 2015. RMS of 1.3 with a 3% noise floor.

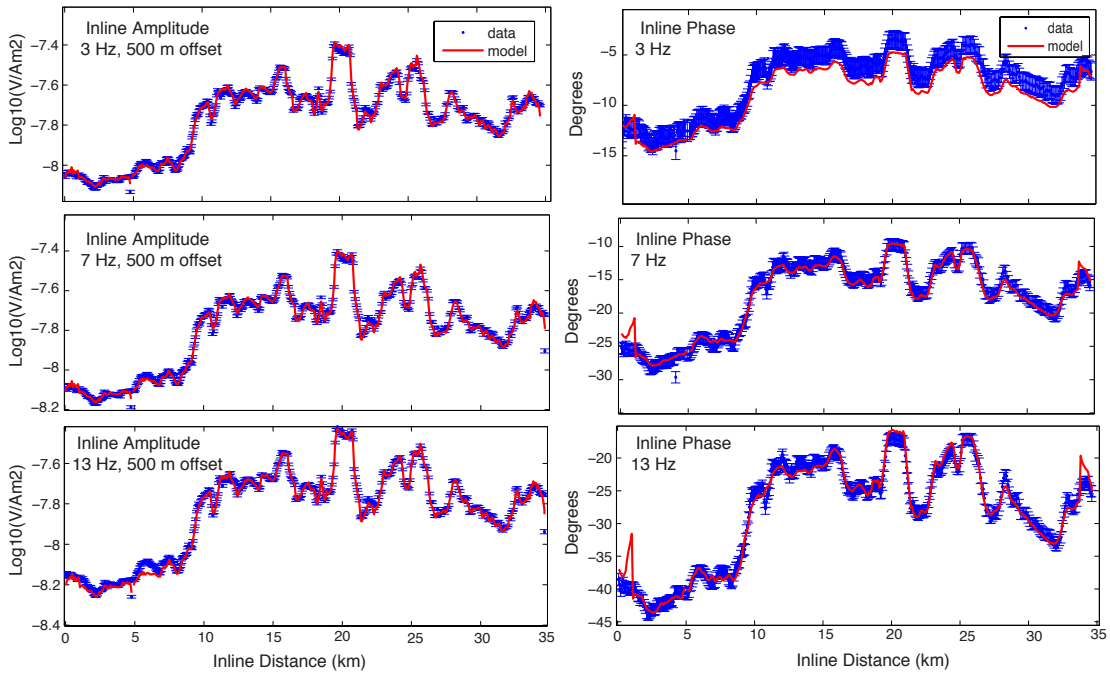

Figure 18: Line fits of data and model response from amplitude and phase anisotropic inversion for all frequencies from Tow 3 in 2015 for the 500 m offset Porpoise.

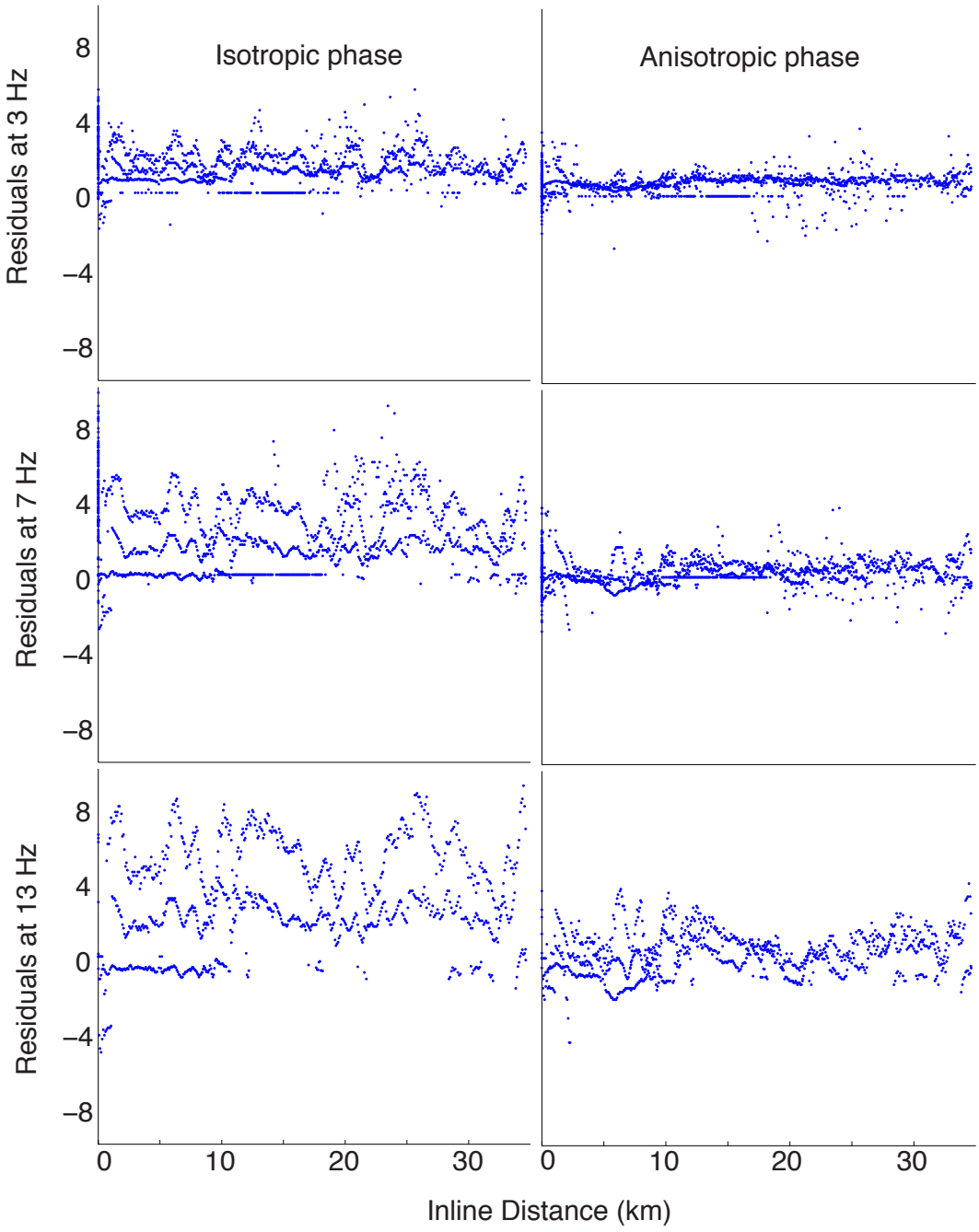

Figure 19: Comparison of residuals from anisotorpic and isotropic models of Tow 3. Isotropic inversions residuals on left, anisotropic residuals on right. Note the improvement in bias of residuals when using anisotropic model.

Anisotropic inversions of amplitude and phase data were completed for all tows. Fence plots of the results are shown in Figures 20 and 21. Vertical resisitivty shows the top of a resistive layer, but often struggles to resolve the bottom. The anisotropy ratio, however, reveals both top and bottom boundaries. It is known that gas hydrade forms in layers which results in electrical anisotropy (*Fredrick and Buffet*, 2013), and it is conceivable that ice preferencially freezes in one lithology, leaving behind a brine in another. Layers of resistivie ice interbedded with brackish pore fluid would explain the high anisotropy ratios we see in Figure 21.

Vertical resistivity indicates maximum resistivites of near 300 Ωm, with average permafrost regions having values between 60-100 Ωm. High resistivity values are found offshore the Sag River and further east. This highly resistive zone further east is near the outflow of a smaller stream than the Sag and also near a small island, both the local hydrology and local topography in this area are likely serving to preserve permafrost. Anisotropy ratio indicates permafrost is buried 100-200 m deep and extends to between 400 m and 600 m. Offshore the Sag River the upper bound is extended upward and indicates permafrost starting within tens of meters of the surface. Between the Sag River and the other region of high vertical resistivity there is an area with resistivities higher than marine sediment, but no anisotropy signature, which likely means the resisitve layer is due to something else, such as freshening of the pore water from the Sag river outflow.

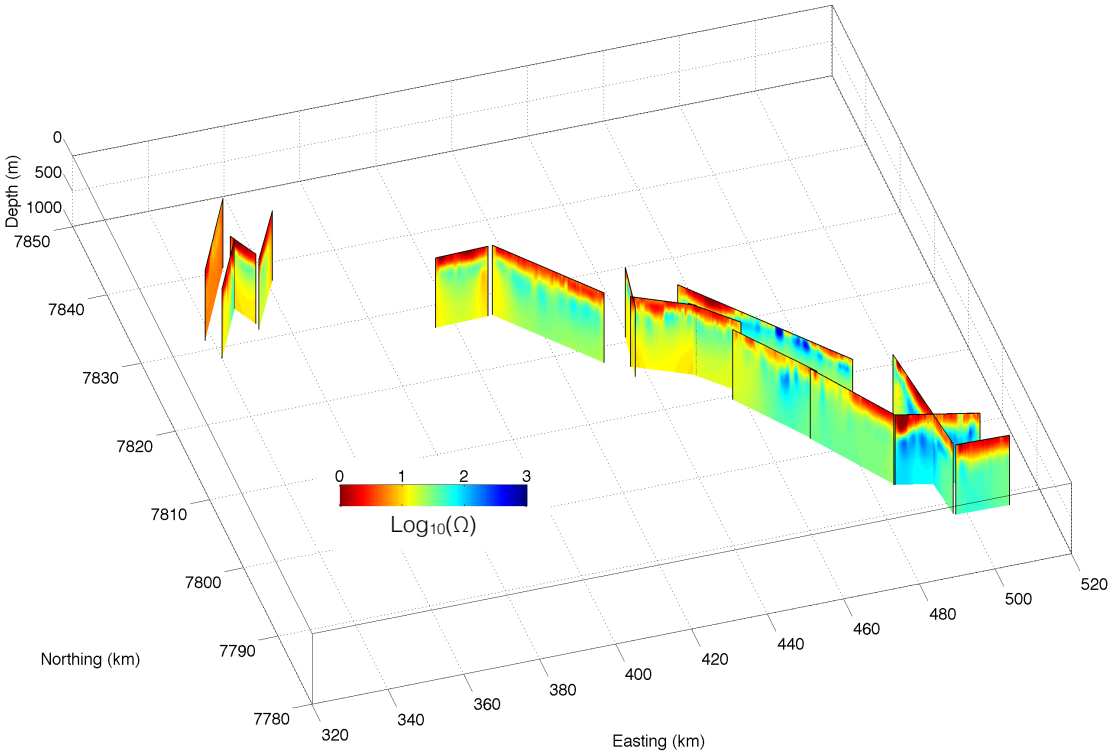

Figure 20: Fence plot of vertical resistivity for 2015.

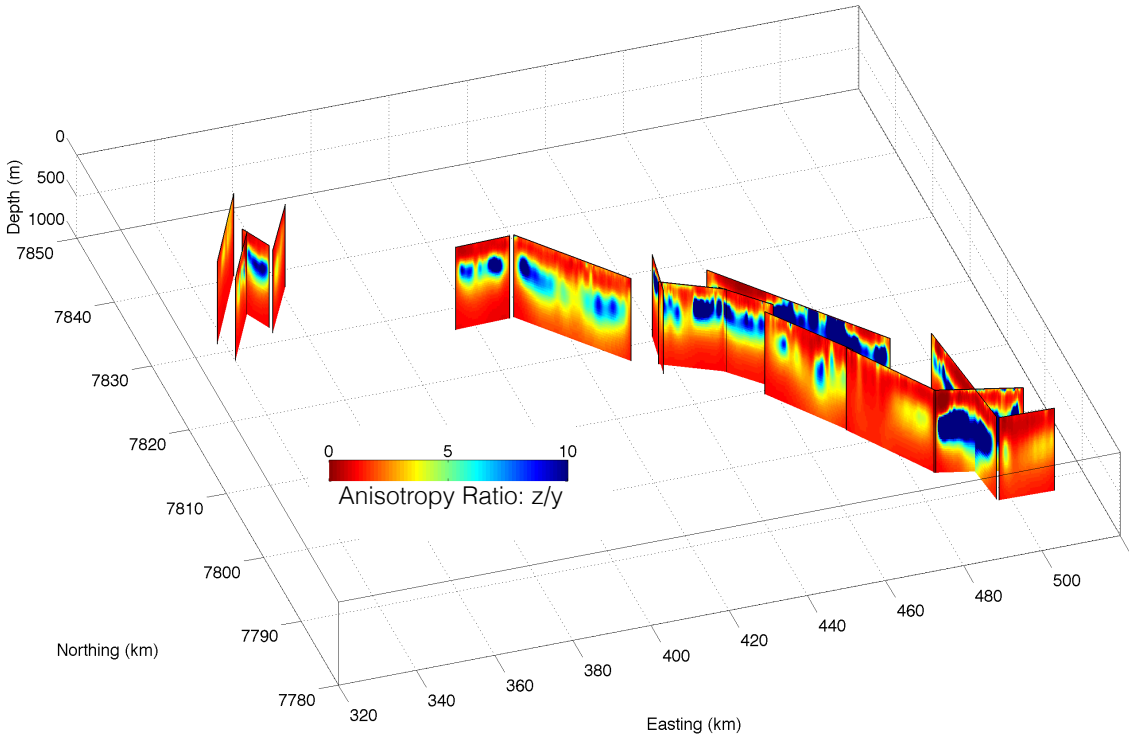

Figure 21: Fence plot of anisotropy ratio for 2015.

From 2014 we have a shore perpendicular tow that begins near the Sag River and extends to the barrier islands, which is near the seismically inferred edge of permafrost. An amplitude only isotropic inversion is shown in Figure 22 with model fits in Figure 23. The resistive permafrost layer is thickest near shore and thins offshore, and appears to be melting mostly from the bottom as saltwater intrudes beneath the frozen layer.

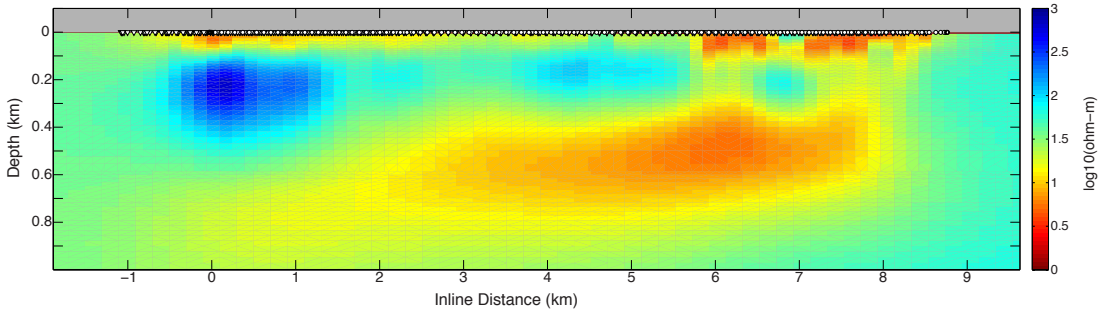

Figure 22: Shore perpendicular profile, fits to an RMS of 1.5 with a 3% noise floor. Left side of model is near shore at the Sag River outflow and the right side is offshore near the barrier islands.

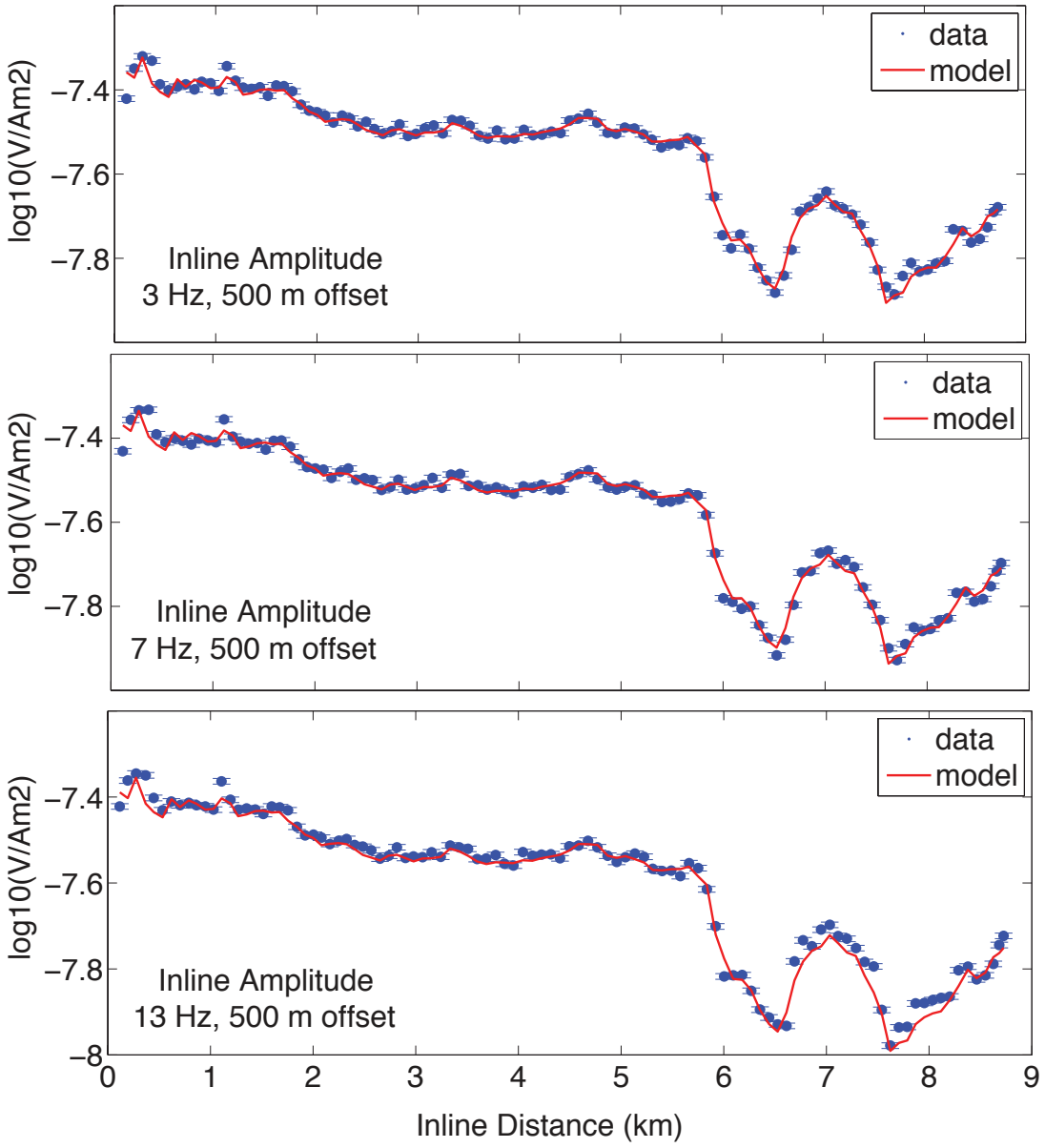

Figure 23: Shore perpendicular profile model fit to data for the 500 m offset Porpoise in 2014. No phase data available for this year.

4.2 Seafloor receiver results

Seafloor receivers were included in a few locations to gather data at longer (>1km) offsets and potentially image deeper beneath the base of permafrost. Three seafloor receivers were located on Tow 4, which is closer to shore than Tow 3 and spans the eastern half of the Sag River. Amplitude only isotropic inversions, as well as amplitude and phase isotropic and anisotropic were run for the seafloor receivers. Both isotropic inversions only fit to an RMS of 2.0 with a 3% noise floor, but the anisotropic model was able to fit amplitude and phase to an RMS of 1.4 with the same 3% noise floor. The Porpoise anisotropic inversion is shown in Figure 24 along with fits at all frequencies for the 500 m offset Porpoise in Figure 25 and the seafloor receiver aniostropic inversion is in Figure 26 with model fits in Figure 27.

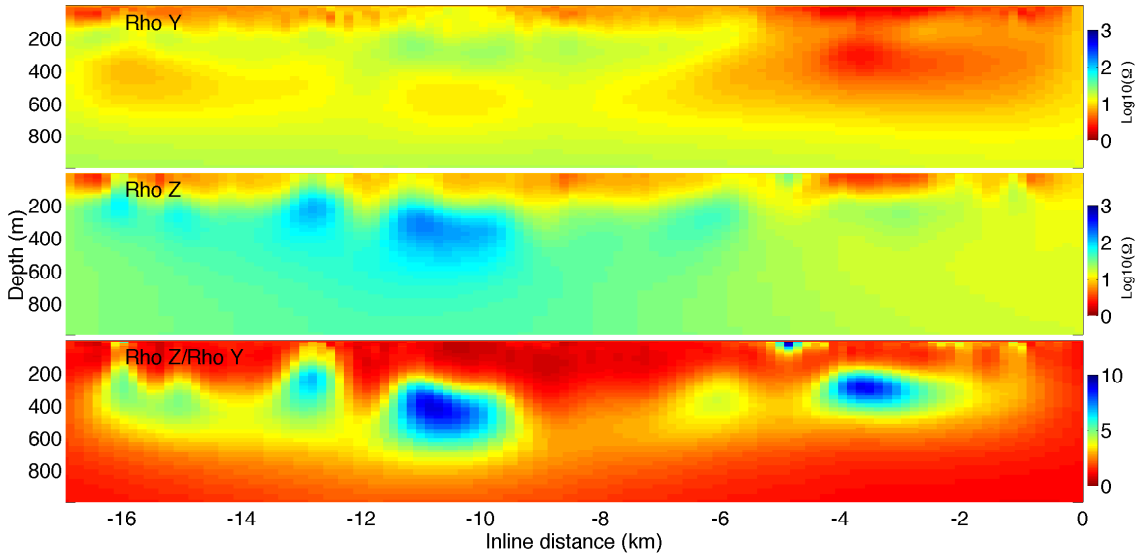

Figure 24: Amplitude and phase anisotropic inversion using Porpoises from Tow 4 in 2015.

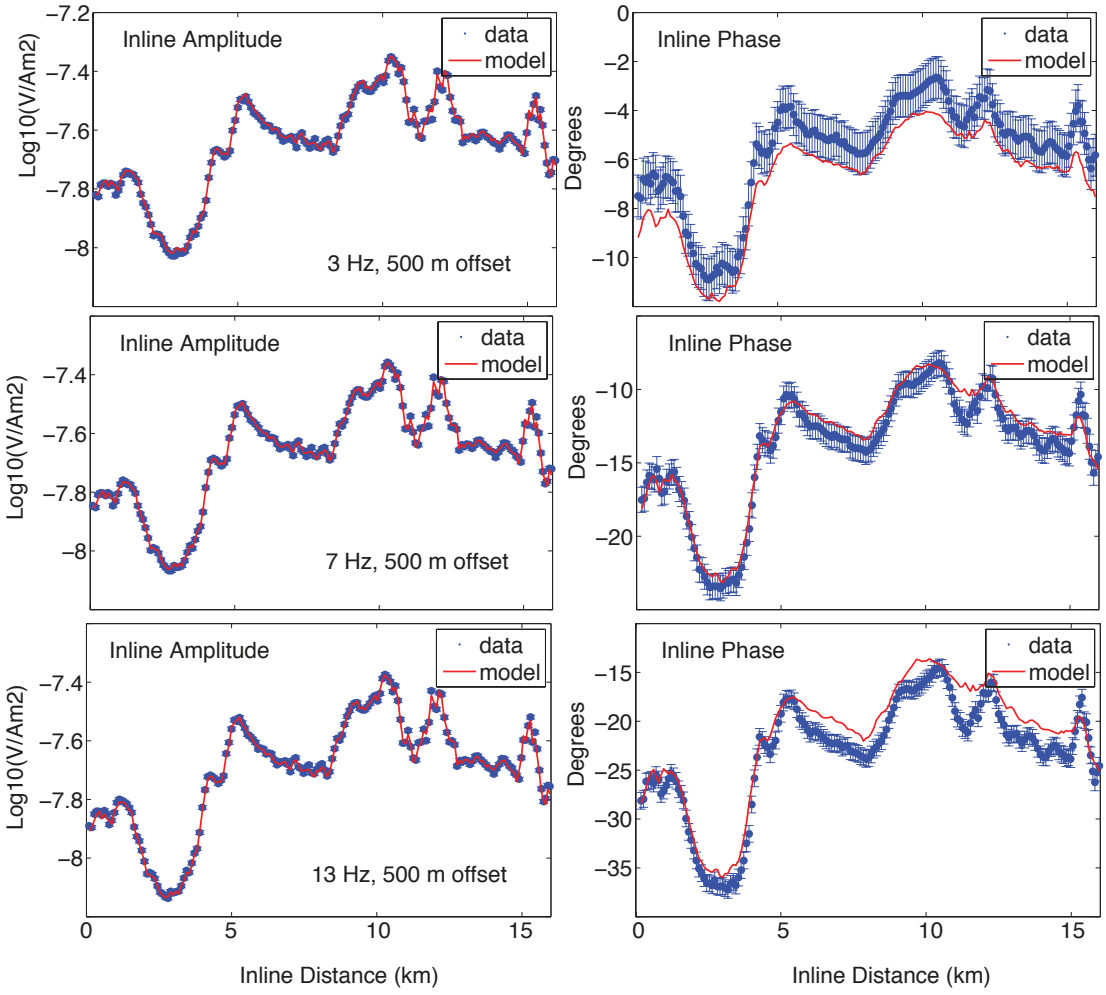

Figure 25: Line fits of data and model response from amplitude and phase anisotropic inversion at 3 Hz from Tow 4 in 2015, 500 m offset Porpoise.

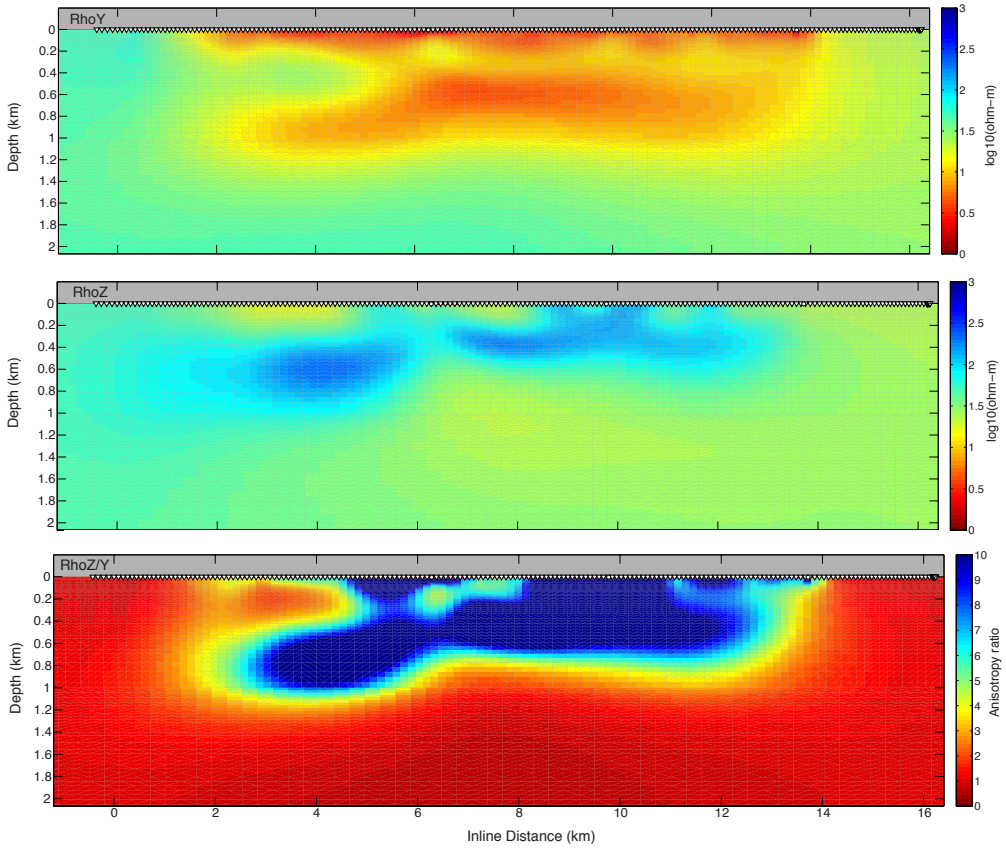

Figure 26: Amplitude and phase anisotropic inversion from seafloor receivers located on Tow 4 in 2015.

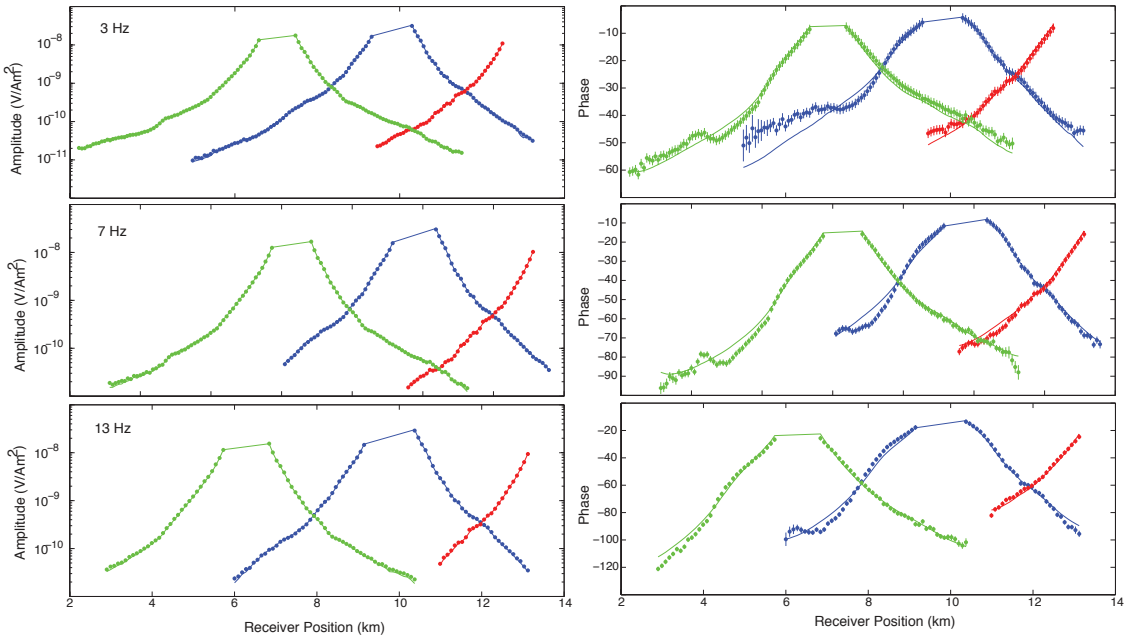

Figure 27: Line fits of data and model response from amplitude and phase anisotropic inversion at 3 Hz from seafloor receivers located on Tow 4 in 2015.

5 Interpretation and conclusions

Our surface towed CSEM system was successful at characterizing resistivity to a depth of about 800 m in 1-10 m water depths offshore Prudhoe Bay. Apparent resistivity in the region ranged from 1 Ωm, a value typical of marine sediments, to over 100 Ωm, which we interpret as ice-bonded permafrost. In areas with seismically inferred permafrost, apparent resistivity varied from 10 Ωm to over 100 Ωm, indicating that there is both ice-bearing and ice-bonded permafrost offshore Prudhoe Bay. Because CSEM and seismic refraction methods are sensitive to different physical phenomena, we do not expect them to yield identical information. Strong seismic refractions occur when there is a sharp velocity increase while the CSEM method is more sensitive to the total ice fraction. In the region of the Sag River outflow, a seismic refraction survey (*Brothers et al.*, 2012) measured an increased p-wave velocity ($V_p > 2.8$km/s) where the CSEM results show resistive anomalies over 100 Ωm. Together, these observations indicate an extensive amount of ice-bonded permafrost correlated with the river outflow. Seismic refraction data continues to see elevated p-wave velocities (V_p>2.8 km/s) from northwest of the Sag River through Harrison Bay, while the resistivity values decrease to between 60 and 100 Ωm. CSEM inversions show a resisive permafrost layer from the surface to 600 m depth offshore Prudhoe Bay and a thinner layer from 250 m to 400 m depth in Harrrison Bay which is in agreement with the thinning trend from Prudhoe Bay to Harrison Bay seen in onshore permafrost.

In contrast, to the immediate southeast of the Sag River, seismic refraction data detected lower velocity increases ($V_p > 2.3$ km/s) consistent with ice-bearing, but not ice-bonded permafrost. CSEM results show a decrease in resistivity and a gap in anisotropy ratio in this region, indicating the resistivity anomaly may be from a different source, i.e. freshening of porewater fluids. Ice-bonded permafrost is impermeable to water, so any ground water needs to flow under or around the ice-bonded permafrost. The southeast side of the Sag River is the side without ice-bonded permafrost (*Brothers et al.*, 2012) and therefore where fresh groundwater can flow and freshen the pore fluid. Fresh pore fluid beneath the permafrost layer may affect our ability to detect the base of permafrost using resistivity alone. Anisotropy seems to be the remedy to this because fresh water saturated sediments will be isotropic while the frozen sections will be anisotropic.

6 Research Products

Seminars, conference presentations, etc.

AGU fall meeting December 2015

Scripps Seafloor Electromagnetic Methods Consortium Sponsors Workshop, La Jolla, CA, March 2015

Electromagnetic Induction Workshop, Chiangmai, Thailand, August 2016

Publications

Sherman, D., P. Kannberg, S. Constable (2016) Surface towed electromagnetic system for mapping subsea Arctic permafrost, *Earth and Planetary Science Letters*, in press.

Martin, T. P. (2015). Mapping Porosity Structure Offshore Torrey Pines State Natural Reserve and Del Mar, California Using a Surface Towed EM System. UC San Diego: b8887341.

7 Appendix

Appendix of all anisotropic models from lines towed in 2015, excepting those shown previously.

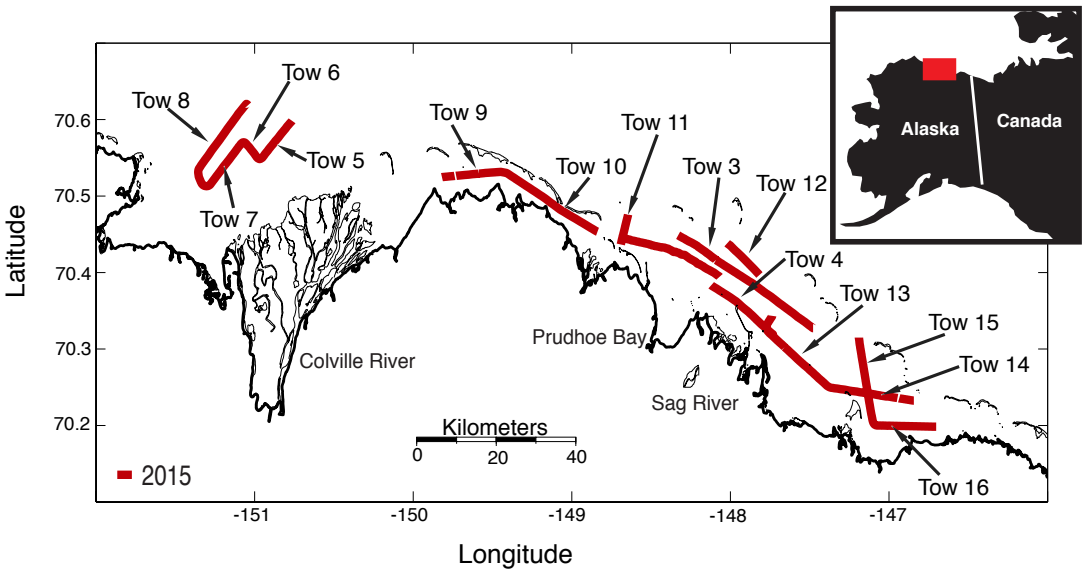

Figure 28: Map of labelled tow lines from 2015.

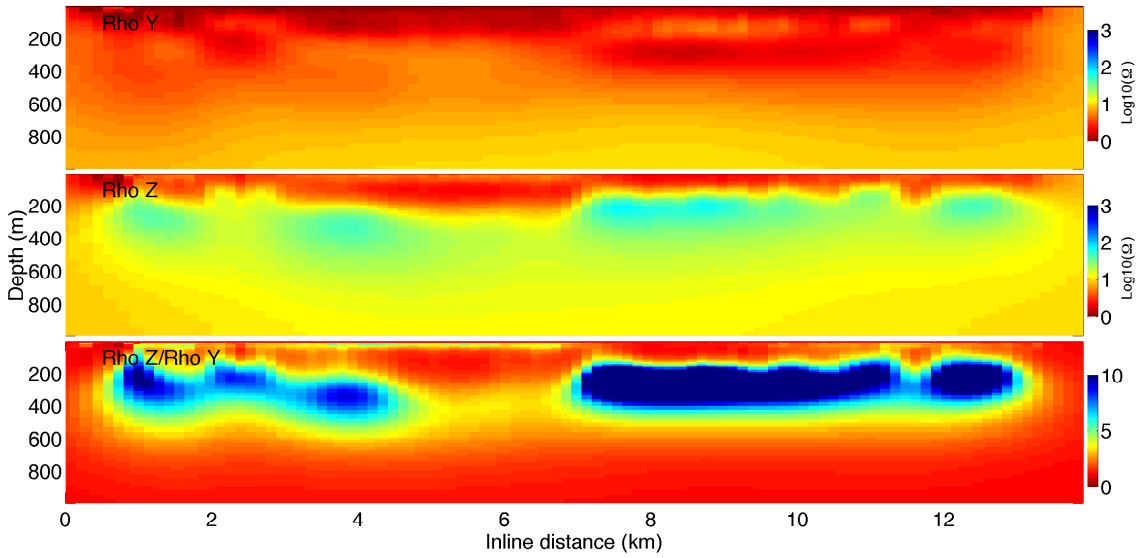

Figure 29: Anisotropic model of amplitude and phase data for Tow 1 in 2015. Fit to an RMS of 1.0 with a 3% noise floor.

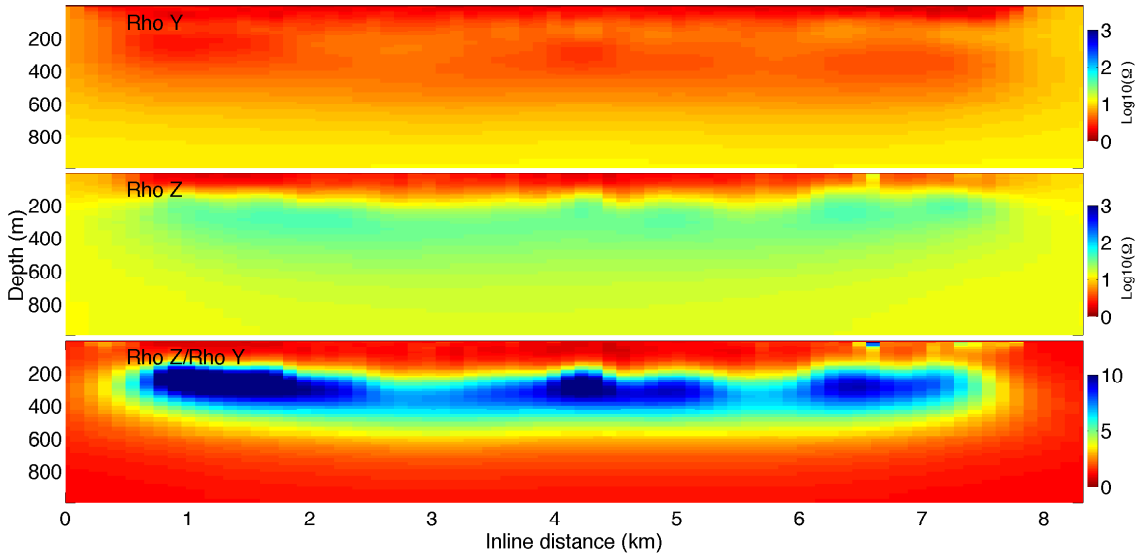

Figure 30: Anisotropic model of amplitude and phase data for Tow 2 in 2015. Fit to an RMS of 1.0 with a 3% noise floor.

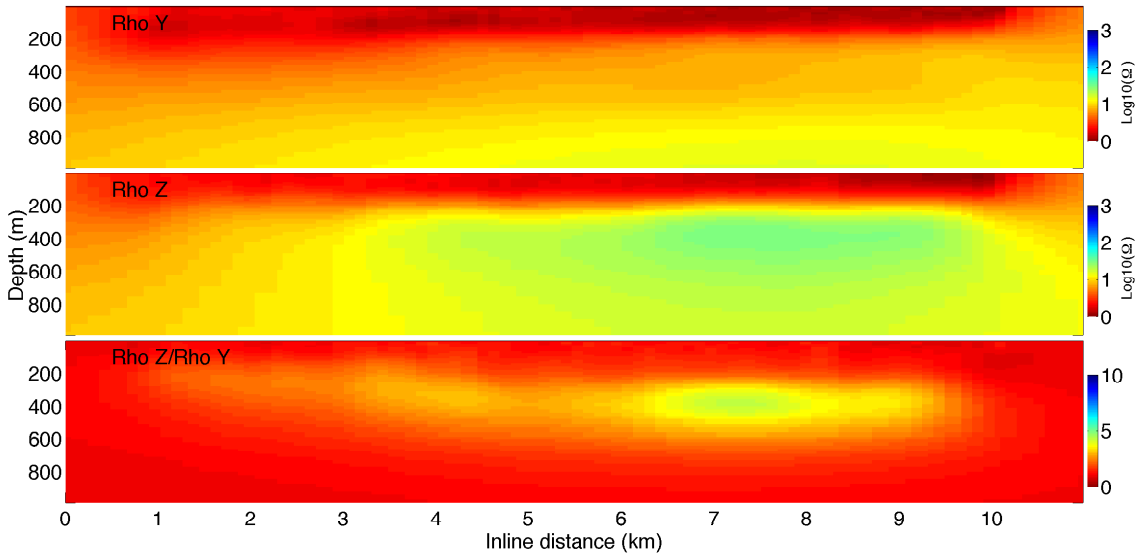

Figure 31: Anisotropic model of amplitude and phase data for Tow 5 in 2015. Fit to an RMS of 1.0 with a 3% noise floor.

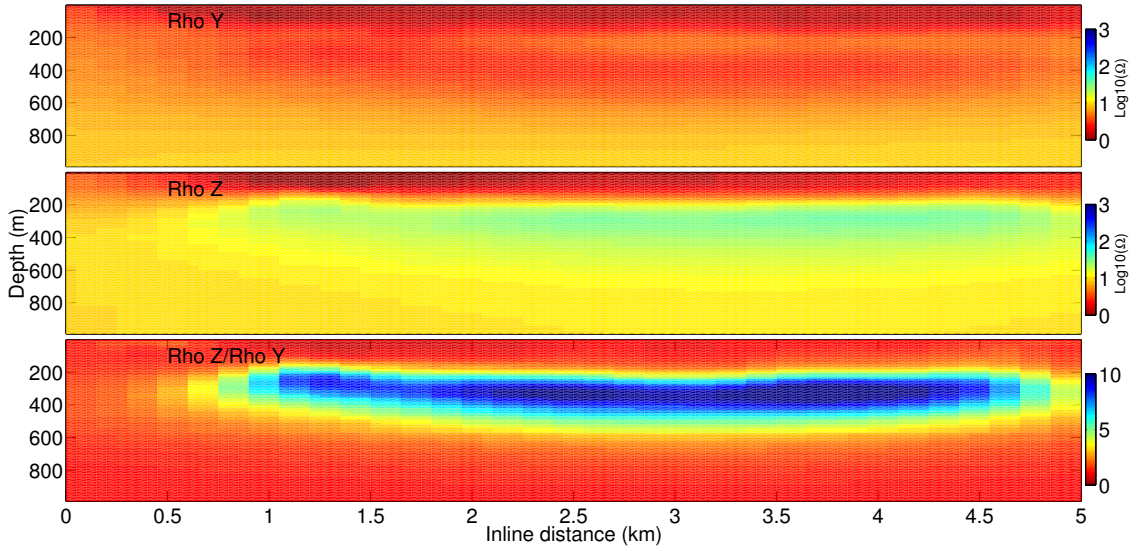

Figure 32: Anisotropic model of amplitude and phase data for Tow 6 in 2015. Fit to an RMS of 1.0 with a 3% noise floor.

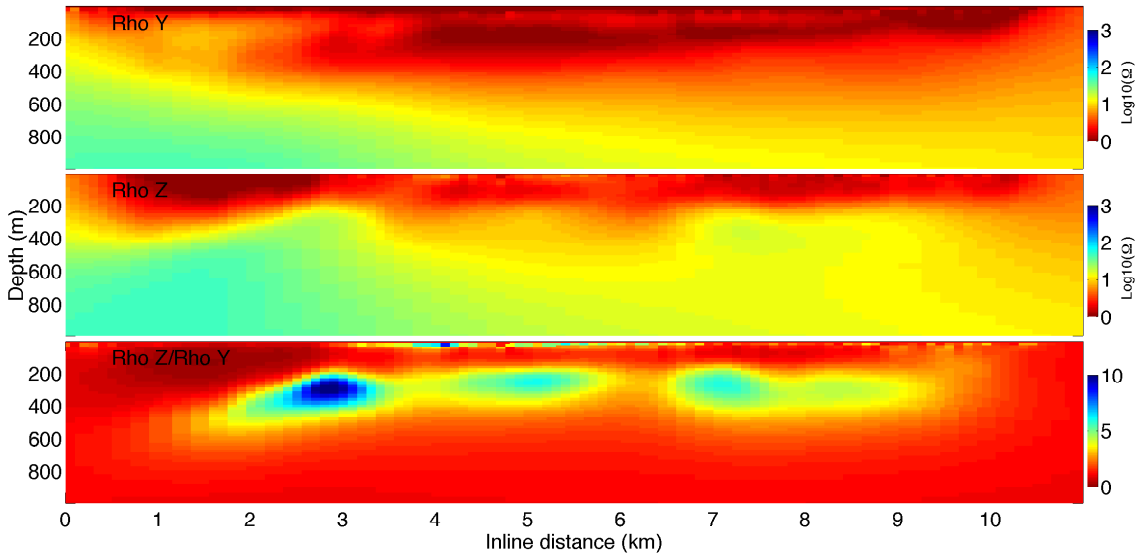

Figure 33: Anisotropic model of amplitude and phase data for Tow 7 in 2015. Fit to an RMS of 1.0 with a 3% noise floor.

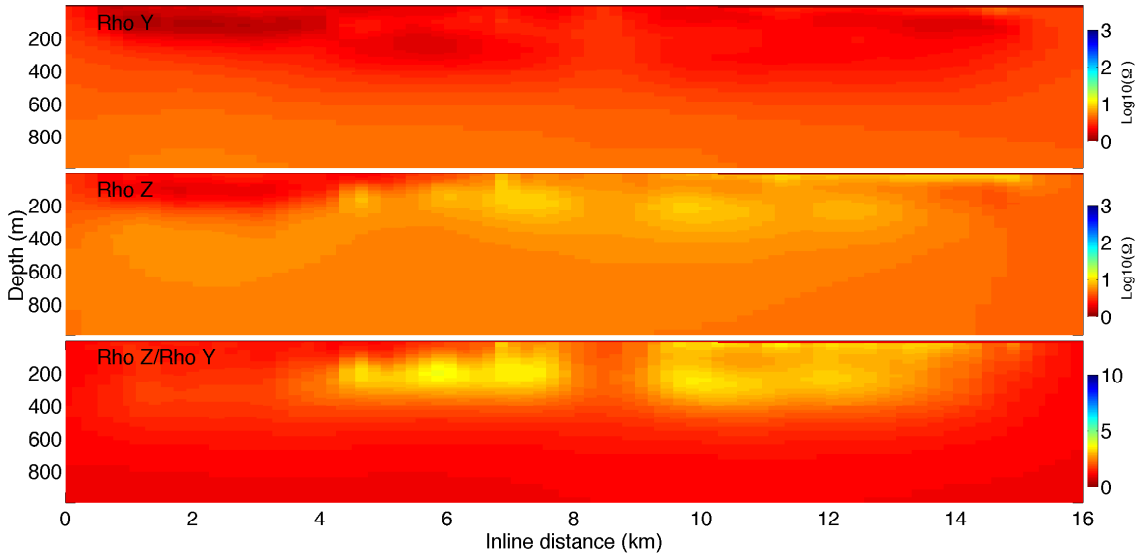

Figure 34: Anisotropic model of amplitude and phase data for Tow 8 in 2015. Fit to an RMS of 1.0 with a 3% noise floor.

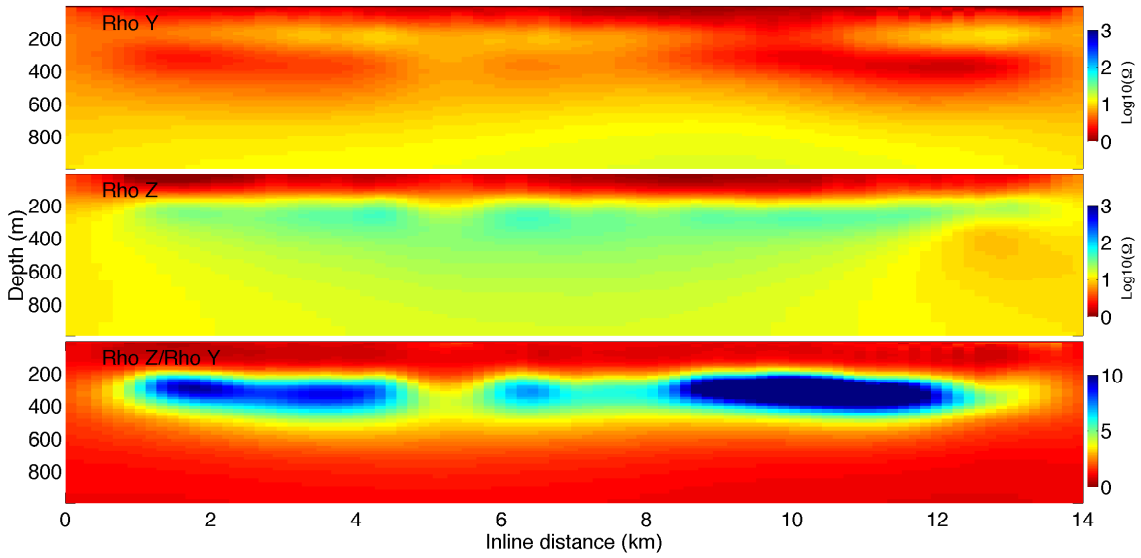

Figure 35: Anisotropic model of amplitude and phase data for Tow 9 in 2015. Fit to an RMS of 1.5 with a 3% noise floor.

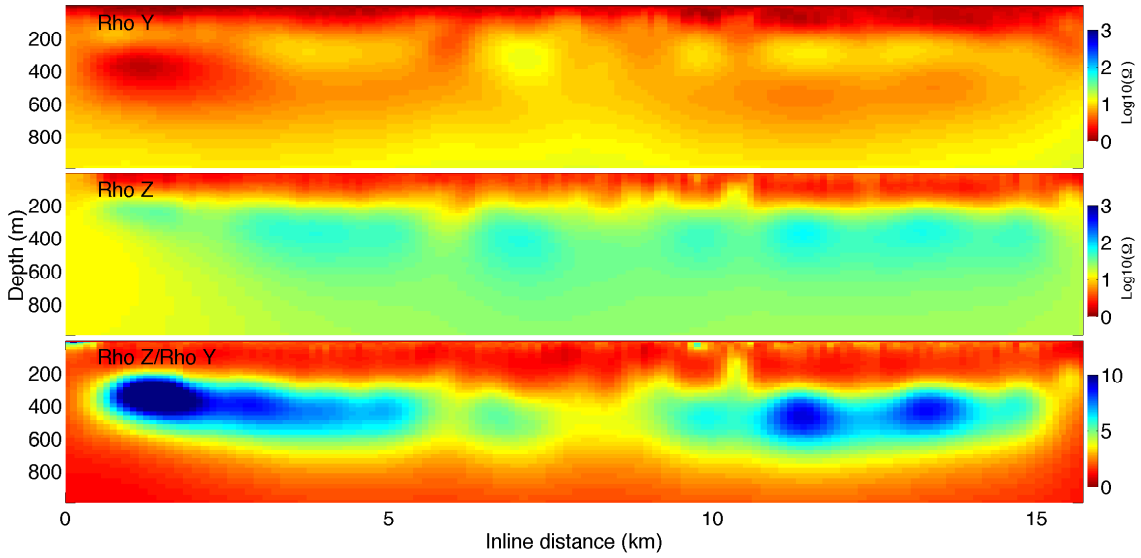

Figure 36: Anisotropic model of amplitude and phase data for Tow 10 in 2015. Fit to an RMS of 1.0 with a 3% noise floor.

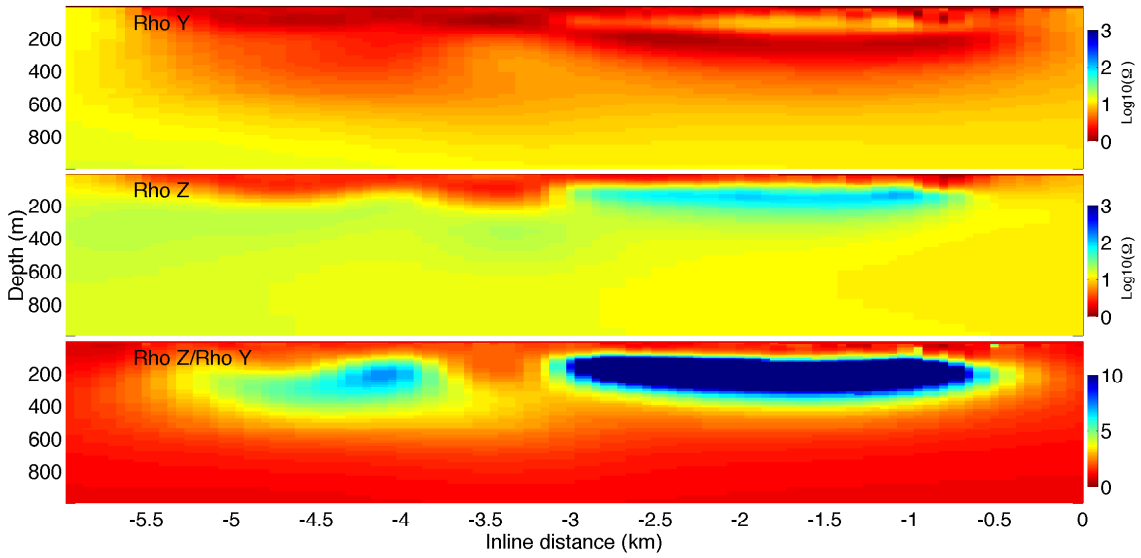

Figure 37: Anisotropic model of amplitude and phase data for Tow 11 in 2015. Fit to an RMS of 1.0 with a 3% noise floor.

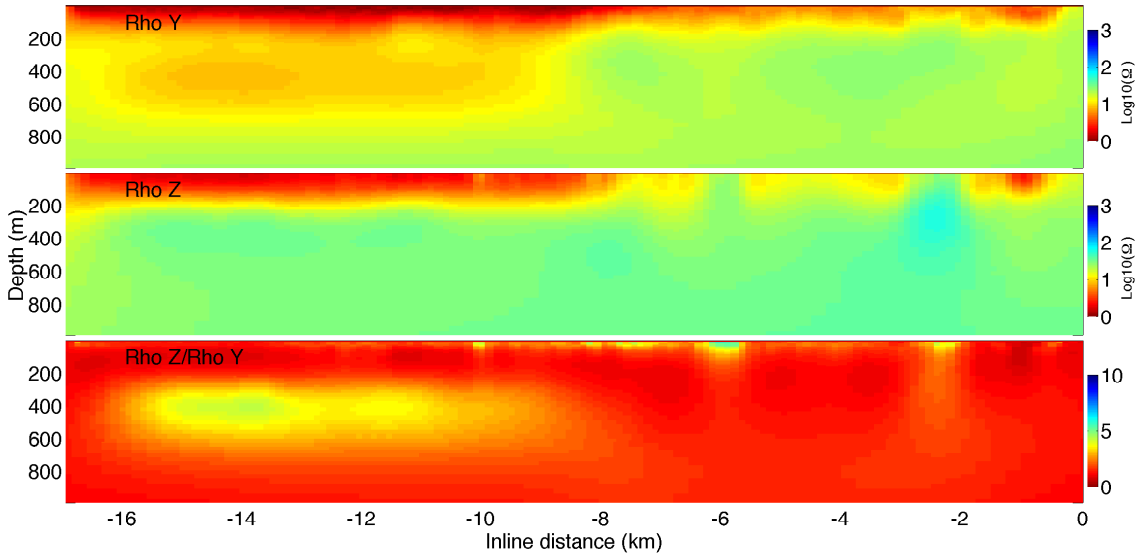

Figure 38: Anisotropic model of amplitude and phase data for Tow 13 in 2015. Fit to an RMS of 1.0 with a 3% noise floor.

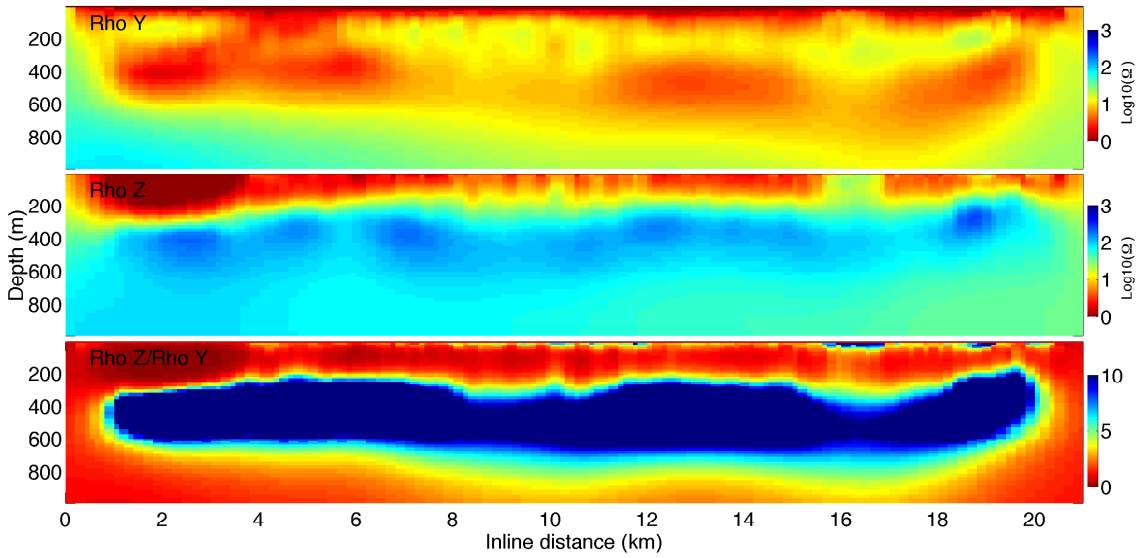

Figure 39: Anisotropic model of amplitude and phase data for Tow 14 in 2015. Fit to an RMS of 1.0 with a 3% noise floor.

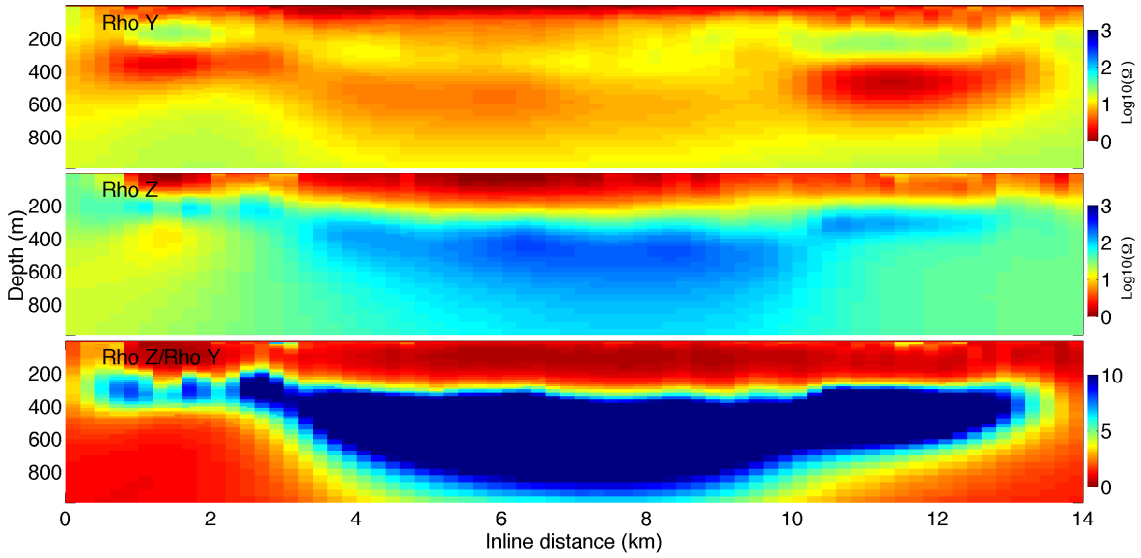

Figure 40: Anisotropic model of amplitude and phase data for Tow 15 in 2015. Fit to an RMS of 1.5 with a 3% noise floor.

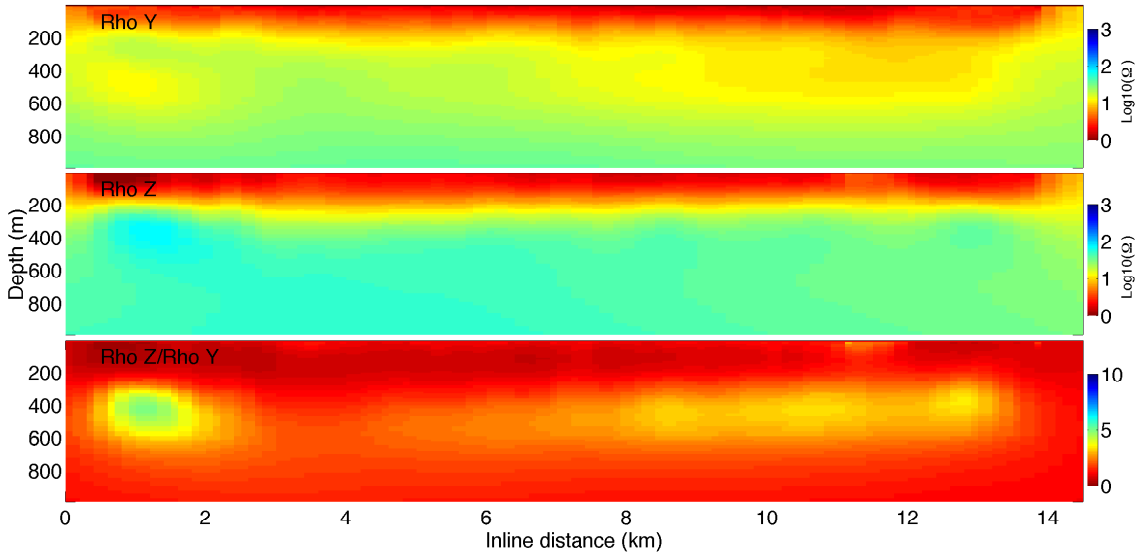

Figure 41: Anisotropic model of amplitude and phase data for Tow 16 in 2015. Fit to an RMS of 1.3 with a 3% noise floor.

References

[1] Brothers, L. L., P. E. Hart, and C. D. Ruppel (2012), Minimum distribution of subsea ice-bearing permafrost on the U.S. Beaufort Sea continental shelf, *Geophys. Res. Lett.*, *39*, L15501.

[2] Collet, T. S., L.W. Myung, W. F. Agena, J. J. Miller, M. V. Lewis, R. Boswell, T. L. Inks (2011) Permafrost-associated natural gas hydrate occurrences on the Alaskan North Slope, *Mar. Pet. Geol.*, *28*, 279-294

[3] Collett, T.S., K.J. Bird, K.A. Kvenvolden, and L.B. Magoon (1989), Map showing the depth to the base of the deepest ice-bearing permafrost as determined from well logs, North Slope, Alaska: USGS Oil and Gas Investigations Map 222.

[4] Constable, S. C., P. Kannberg, K. A. Weitemeyer (2016) Vulcan: A deep-towed CSEM receiver, *Geochem. Geophy. Geosy.*, *17*, 1042-1064

[5] Daniels, J.J., G.V. Keller, and J.J. Jacobson (1976) Computer-assisted interpretation of electromagnetic soundings over a permafrost section. *Geophysics. 41*(4) 752-765

[6] Frederick, J. M., and B. A. Buffett (2015), Effects of submarine groundwater discharge on the present-day extent of relict submarine permafrost and gas hydrate stability on the Beaufort Sea continental shelf. *J. Geophys. Res. Earth Surf.*, *120*, 417432

[7] Frederick, J. M., and B. A. Buffett (2014), Taliks in relict submarine permafrost and methane hydrate deposits: Pathways for gas escape under present and future conditions, *J. Geophys. Res. Earth Surf.*, *119*, 106 -122

[8] Johansen, T. A., P. Digranes, M. van Schaack, and I. Lonne (2003), Seismic mapping and modeling of near-surface sediments in polar areas, *Geophysics*, *62*(2), 1-8

[9] Key, K. W. (2016). MARE2DEM: a 2-D inversion code for controlled-source electromagnetic data. *Geophys. J. Int.*, *207*, 571-588

[10] Martin, T. P. (2015). Mapping Porosity Structure Offshore Torrey Pines State Natural Reserve and Del Mar, California Using a Surface Towed EM System. UC San Diego: b8887341. Retrieved from: http://escholarship.org/uc/item/45p0062c. Accessed on May 2, 2016.

[11] Myer, D., S. C. Constable, K. W. Key (2010), Broad-band waveforms and robust processing for marine CSEM surveys. *Geophys. J. Int.*, *184*, 689-698.

[12] Osterkamp, T. E., (2001) Sub-sea permafrost in Encyclopedia of Ocean Sciences (Second Edition), pp 559-569, Academic Press.